LA-UR-14-20201
Approved for public release; distribution is unlimited.

Title: Thermal and Physical Properties of Plutonium Dioxide Produced from the Oxidation of Metal: a Data Summary

Author(s): Wayne, David M.

Intended for: Data repository for access by other DOE Laboratories

Issued: 2014-01-13

Thermal and Physical Properties of Plutonium Dioxide Produced from the Oxidation of Metal: a Data Summary

David M. Wayne
Los Alamos National Laboratory
MET-1, MS E-511, Los Alamos, NM 87545

ABSTRACT

The ARIES Program at the Los Alamos National Laboratory removes plutonium metal from decommissioned nuclear weapons, and converts it to plutonium dioxide in a specially-designed Direct Metal Oxidation furnace. The plutonium dioxide is analyzed for specific surface area, particle size distribution, and moisture content. The purpose of these analyses is to certify that the plutonium dioxide powder meets or exceeds the specifications of the end-user, and the specifications for the packaging and transport of nuclear materials. Analytical results from plutonium dioxide from ARIES development activities, from ARIES production activities, from muffle furnace oxidation of metal, and from metal that was oxidized over a lengthy time interval in air at room temperature, are presented. The processes studied produce plutonium dioxide powder with distinct differences in measured properties, indicating the significant influence of oxidation conditions on physical properties.

INTRODUCTION

During the course of the Advanced Recovery and Integrated Extraction System (ARIES) production effort at LANL, we have undertaken a variety of testing methods to certify that the PuO_2 product meets the specifications outlined in the Plutonium Interface Control Document [1]; hereafter referred to as the ICD. The ARIES oxide product is sealed in welded containers and shipped per the requirements and specifications in DOE-STD-3013 [2]. To address the requirements of both the ICD and of DOE-STD-3013, we devised a powder processing and assessment regimen for ARIES oxides to guarantee a homogenous oxide product with uniform chemical and physical properties. To date, over 50 oxide lots have been produced and analyzed in preparation for shipping to the Savannah River Site (SRS) in DOE-approved, welded 3013 containers.

Measurement of the particle size distribution (PSD) and specific surface area (SSA) of PuO_2 powders from different process streams has been performed at the Los Alamos National Laboratory (LANL) for several decades. Due to programmatic requirements, ARIES oxides are quite well-characterized; perhaps more so than other actinide oxide products. In addition to the materials evaluated for the present study, the physical and chemical properties of PuO_2 produced during the 1st and 2nd ARIES Demonstrations have also been documented and discussed [3, 4]. Before ARIES entered the production phase in 2010, the United States Department of Energy specified that the moisture content of plutonium-bearing materials destined for interim storage in 3013 containers per DOE-STD-3013 be quantified by thermogravimetric analysis (TGA) coupled either with quadrupole mass spectrometry (TGA-MS) or Fourier Transform Infrared Spectroscopy (TGA-FTIR). At LANL, TGA-MS analyses are routinely performed to assess moisture levels in Pu-bearing materials.

For Pu-bearing materials to be shipped to SRS, a 20 Points agreement [5] details the manner in which LANL meets the requirements of DOE-STD-3013 for all aspects of Pu oxide stabilization, sampling, packaging, and analysis. All TGA-MS analyses of PuO_2 must adhere to these collective guidelines, which include:

1. Heating to at least 1000°C at a rate of 20°C or less per minute.
2. The use of ultra-high-purity argon (99.999%) or helium (99.99%) carrier gas.
3. The sample measured must be ≥ 3 g.
4. Both mass numbers 17 (OH) and 18 (H_2O) must be used to measure moisture.

THE ARIES OXIDE PROCESS STREAM IN PF-4

The ARIES project comprises a process line that disassembles plutonium-containing components from nuclear weapons, extracts the Pu metal, converts the metal to oxide, and processes that oxide for transport to the Savannah River Site (SRS) in welded 3013 containers [1, 2]. Two versions of the Direct Metal Oxidation (DMO) Furnace have been used to produce actinide oxides from metal during ARIES testing and development. The 1st ARIES Demonstration was performed during the late 1990s using a stainless steel furnace adapted from the HYDOX furnace which was intended to convert Pu metal to Pu hydride or Pu nitride intermediaries prior to oxidation. The HYDOX furnace was retrofitted to eliminate the hydride- and nitride-forming capabilities, hence the name “Direct Metal Oxidation” furnace.

The first DMO unit (DMO-1) oxidized the metal in a rotating, perforated basket within a controlled, O_2-rich atmosphere at ~600°C. Various O_2-He gas mixtures were tested to facilitate the oxidation reaction in the furnace. The rapidly-formed oxide spalled off the metal parts, fell through the perforations and into a fritted quartz tube which served as a gas inlet, oxide reservoir, and calcination furnace. Though calcination was available, only a few of the oxide batches were calcined, and in those the calcination typically only went to ~600°C. The same DMO furnace setup was used for the 2nd ARIES Demonstration during the early 2000s. No records were retained concerning the calcination of oxide produced during the 1st and 2nd ARIES Demonstrations. With the exception of the material used in developing the ARIES NDA Standard [4], oxide lots produced during these demonstrations were only subjected to a brief (ca. 10-20 minutes) interval of rod milling prior to storage.

All production-scale (UPOPLOT) oxide, and all ARIES testing and development from 2009 to the present has taken place in the DMO-2 Furnace, a redesigned and improved version of the DMO-1 furnace. In DMO-2, oxidation is maintained between 475 and 575°C in an optimized helium – oxygen mixture (75% O_2 / 25% He) flowing into the reaction zone at 2.0 L/ min (i.e., 1.5 L/min O_2 and 0.5 L/min He). The total amount of O_2 available for Pu oxidation exceeds that needed to produce stoichiometric PuO_2. Oxide chips and powder are collected and calcined for 130 to 135 minutes at 950-1040°C in the same He-O_2 atmosphere.

The ARIES / UPOPLOT product oxide is then sieved to separate powder that is already less than 180 um. The oversized material is iteratively milled and sieved so that ~90-99% of the final product passes through a 180 μm sieve. The fully-processed powder lot is then homogenized by mechanical blending, sampled for analysis, and packaged to meet the requirements of DOE-STD-3013. Analytical samples are extracted from the fully processed ARIES oxide shortly after homogenization. ARIES oxides are essentially pure single-phase materials with Pu > 86%, and relatively consistent trace and minor element contents. The primary elemental impurities are Ga and Am inherited from the Pu source material, plus trace amounts of C, Fe, Ni, and other elements that are mostly by-products of material processing [4].

OTHER OXIDATION MODES: PASSIVE OXIDATION AND MUFFLE FURNACE TESTING

We obtained one 15 gram sample of Pu oxide directly from the ARIES Disassembly Team. This oxide was taken from a defective 35-year-old weapon pit that had slowly oxidized at ambient conditions over an undetermined time span. This oxide consists of a very fine, flour-like powder that was analyzed with no pretreatment other than riffling to reduce the sample size.

We have also examined a set of samples that were oxidized in ambient air in a muffle furnace. The formalized Muffle Furnace Test Plan (MFTP) specifies that Pu metal be oxidized in an aluminosilicate boat for at least 12 hours at 500°C followed by stabilization of the converted oxide at 950°C for at least two hours. Ultimately, the MFTP was devised to demonstrate that static oxidation and calcination in a muffle furnace could yield plutonium oxide that meets the requirements of ICD-08-025-02 (G-ESR-K-00039, Rev 2), “LANL-SRS Plutonium Dioxide Powder Interface Control Document,” and those of the “20 points” requirements necessary to meet G-ESR-G-00035 for the shipment and eventual storage of material at K-Area under DOE-STD-3013. The MFTP oxide was produced in several smaller batches and each batch was

subjected to the full range of available physical and thermal characterization techniques, including PSD, SSA, and TGA-MS. Then, the individual MFTP batches were sieved, milled, blended, and sampled using the same procedure implemented for the ARIES DMO-2 oxides. The fully processed MFTP oxide was packaged as UPOPLOT0038M, following sampling, and analysis in the same manner as the ARIES DMO oxide lots.

SAMPLING, ANALYTICAL METHODS AND INSTRUMENTATION

Table 1 is a summary of sample types and process paths. Different process paths are denoted by an indicator prefix (e.g., UPOPLOT, ARIOX, MFTP, etc.). In all cases the suffix "LT180" refers to the sub-180 μm sieve fraction of the unprocessed oxide.

All equipment and instrumentation used for this study is housed entirely within dry air PF-4 gloveboxes fitted with hard-plumbed, filtered gas inlets, and sealed electrical and telemetric feedthroughs. During production, ambient conditions within the dry air gloveboxes were: temperature (T) = 25 to 32^{o}C, relative humidity (%RH) = 0.0 – 0.5% for UPOPLOT0001 to UPOPLOT0036-1 (Appendix 1). During summer 2012, and through the winter of the same year, multiple positive humidity excursions in both the processing and analytical gloveboxes occurred due to maintenance operations on the PF-4 air drying system (Figure 2). The ambient analytical glovebox %RH measurements during TGA-MS analyses of UPOPLOT0036-2 (duplicate run), -38M, -40 and -45 were 4.3%, 7.0%, 1.4%, and 1.9%, respectively. The analytical glovebox %RH for the remaining samples after UPOPLOT0045 was <0.6% at temperature. All oxide processing and characterization operations are paused if the glovebox relative humidity exceeds 15% [5]. A comprehensive survey of glovebox conditions during sampling and TGA-MS analysis, and the corresponding TGA-MS results, is given in Appendix 1.

Samples for SSA, PSD, and TGA-MS measurements were separated directly from the multi-kilogram bulk oxide lots using a sample thief to isolate a 250 gram master sample. The 250-gram sample was then subdivided into 25 gram, or 3 to 5 gram, aliquots using a rotary riffler. The samples were sealed in Cu-gasketed stainless steel ampoules until they are analyzed. The 25-gram sample is further riffled down to eight 100- to 300-mg sub-aliquots, one or more of which are then used for PSD measurements. The remainder of the 25-gram sample is used for surface area analysis. Oxide destined for shipment in 3013 containers must be evaluated for moisture content by TGA-MS, per DOE-STD-3013. The 3013 samples must be ≥3 grams. Samples from oxide batches not destined for shipment can be any size, and are typically between 1 and 3 grams. For this study, TGA-MS samples are decanted directly from the steel ampoule into the TGA crucible, with no pre-treatment or other preparation.

SSA determinations were performed using a 3-port Beta Scientific / Horiba Surface Analyzer (SA-9603-MP) and ultra-high purity He and N_2 gases on nominal 25 g samples that were outgassed in the analysis cells for a minimum of 4 hours at 200^{o}C. We ran either NIST SRM 1899 or NIST SRM 1900 concurrently with two PuO_2 samples. The variation of the measured SSA values of the SRMs was typically ≤5% relative standard deviation (RSD) from the certified value, and was always within <10% RSD. PSD measurements were carried out using a Horiba LA-920 laser diffraction particle size analyzer. Riffled 100 to 300 mg samples were analyzed 6 to 8 times in rapid succession after a 10 second ultrasonic agitation. In order to counteract the effect of particle settling, the suspension was further agitated between each run using the on-

board ‘de-bubble’ option which further sonicates the fluid and increases its circulation rate for 30 seconds. Analyses were performed using the ‘sequence file’ option which ensures identical fluid flow conditions immediately before and during analysis. Results from 6 to 8 individual runs were then averaged. We also measured the PSD of NIST SRM 1982 before and after the PuO_2 sample runs. The deviation of the measured D_{50} (=median) value of the SRM from the certified value was <10% RSD for each sample.

TGA-MS runs were performed in Al_2O_3 crucibles using a Netzsch STA 409PC Luxx TGA/DSC equipped with a heated interface and a heated silica capillary transfer line leading to a Pfeiffer ThermoStar Quadrupole MS (GSD 301T) for offgas analysis. Analyses were conducted in flowing ultra-high-purity (UHP) Ar on 10°C per minute ramp from room temperature up to 1100°C. Per agreement with Savannah River Site [5], the TGA furnace chamber was not evacuated prior to analysis, and the working gas must be UHP argon. Water was quantified using both mass-to-charge (*M/z*) ratios = 17 and 18. Repeat analyses of talc and gypsum were conducted in order to construct a calibration curve (n>6) that relates peak area to the weight loss incurred by talc and gypsum dehydration [6]. Aside from OH and H_2O, several other *M/*z ratios were monitored, including (at different times): 2 (H_2), 4 (He), 15 (NH), 16 (O), 30 (NO), 32 (O_2), 35 (^{35}Cl), 36 (^{36}Ar), 37(^{37}Cl), 44(CO_2), and 48 (SO).

SURFACE AREA AND PARTICLE SIZE RESULTS

Plutonium oxide (PuO_2) produced by metal oxidation at ambient conditions (sample 006) is a fine powder with a unimodal (=1.42 μm) distribution around a mean of 1.99±0.09 um (D_{50}=1.62 um). By contrast, ARIES oxide arrives from the DMO as a granular aggregate, with a very wide range of particle sizes: from over 2000 um, to <1.0 um. Sieve analyses indicate that for typical ARIES DMO material, only 20 to 30 weight % consists of fines <180 μm in diameter (Appendix 2). However, DMO runs after UPOPLOT0039 have a different initial PSD, with <180 μm fines comprising up to 75% by weight of the raw material. Pu oxides from the Muffle Furnace Test Plan (MFTP) also contain granular aggregates prior to processing, though they also have a far higher proportion of <180 μm fines than the typical ARIES DMO oxides (Appendix 2).

The single sample of PuO_2 produced by slow metal oxidation at ambient conditions was analyzed several times and has a SSA of 6.89 m^2/g. High-purity PuO_2 produced from nitrate or chloride solutions via oxalate precipitation followed by calcination at 650°C also results in relatively high-surface area particles [7-8] (Figure 3). The ICD places no bounding conditions on the SSA of ARIES oxide feed. Plutonium oxides originating from the ARIES DMO Furnace are low SSA materials. Surface area and particle size data for all fully-processed UPOPLOT oxide samples is summarized in Appendix 3. SSA and PSD data for ARIES-related oxides such as those from the Muffle Furnace Test Plan, the pre-production DMO-2 Test Plans, and uncalcined, minimally-processed oxides from the first and second ARIES Demonstrations are summarized in Appendix 4. Figure 4 shows that the SSA of processed ARIES oxide increases slightly over the duration of the UPOPLOT production cycle, though nearly all measurements fall in a narrow range between 0.1 and 0.4 m^2/g. Only 5 of 53 processed UPOPLOT samples, Lots 38M (muffle furnace), 41-43, and 50, have SSAs that exceed 0.4 m^2/g. Unprocessed PuO_2 produced from metal oxidized in ambient air using a programmable muffle furnace (e.g., the MFTP samples) are similar in terms of surface area (Figure 3) although some minimally-processed, and possibly

uncalcined, samples from the first and second ARIES Demonstrations have SSAs that exceed 1.0 m^2/g (Figure 3; Appendix 4). The origin of the higher surface area materials (~2 m^2/g) emanating from the DMO-1 furnace during the demonstration phase of the ARIES project is not known. Subsequent ARIES oxides, both processed and unprocessed, from the DMO-2 furnace have had consistent and much lower SSA values (Figure 3).

The ICD specifies that the finished ARIES product shall contain no particles greater than 200 μm in diameter, and that the volume percent of fines smaller than 5 μm in diameter shall be minimized. We subsequently agreed to keep the percentage of sub-5 μm fines below an arbitrary limit of 30 % by volume [1]. Nearly all processed ARIES UPOPLOT samples have a distinctive tri-modal PSD, with modes at 0.73 – 3.16 μm, 10.9 – 18.5 μm, and 41.3 - 63.0 μm (Figure 5). The diameter showing the largest volume fraction in the smallest mode is quite variable, while that of the two larger modes varies by ~10% RSD (1σ) (Appendix 3). For these oxides, most of the variability in the PSD results occurs in the relative heights of the different modes, as opposed to their absolute position. Average PSDs from Lots 1-10, 11-20, 21-30 and 31-39 (excluding 38M) are very similar, while the average PSD from Lots 40-51 is significantly different (Figure 5, Table 2). The PSDs of Lots 1-10, 11-20, 21-30, 31-39, and the muffle furnace products are characterized by a relatively large population of particles ≥35 μm in diameter, and a well-defined population of fine particulates that have a mode between 1.0 and 1.5 μm. By contrast, the average PSD from Lots 40-50 are almost unimodal (Figure 5), with a far greater population of particles in the 5-30 μm range, and fewer particles in the ≥35 μm and ≤4 μm ranges. The smallest particle size mode is poorly-defined (Figure 5) and arrives at significantly higher particle diameter (2.79 μm) than those of the other ARIES processed lots (1.08 – 1.41 μm). Average PSD data from Lots 40-50 also shows significantly smaller median and mean particle sizes than the previous averaged lots (Table 2).

The PSDs of the <180 μm fraction from the unprocessed ARIES DMO oxide, and of the <180 μm fraction of the unprocessed MFTP oxide are nearly identical to those routinely obtained from the processed DMO oxide (Figure 6). Compared to the MFTP oxide, those produced in the DMO furnace show much more variability in the various particle size parameters prior to processing (Figure 7; Appendix 4).

THERMOGRAVIMETRIC ANALYSIS

TGA-MS has been performed on approximately 120 PuO_2 samples of various origins over the past 2.5 years. The oxide generated by long-term exposure of the metal to ambient air had a total mass loss of ~0.70 wt. % (Figure 8). Over 80% of the total mass loss (~0.58 wt. %) from this sample was attributable to H_2O, mostly occurring below 500°C, but persisting to well over 800°C. A very small mass gain occurs above 900-950°C, and persists to the analytical endpoint, 1100°C. If we assume that a monolayer of water molecules on 1 m^2/g of PuO_2 surface weighs 0.21 mg/g [9], the amount of water released from this sample corresponds to ~3.7 monolayers, consistent with H_2O adsorption in a humid environment.

Analyses of processed ARIES oxide samples produce remarkably consistent and highly distinctive results. Within the measurement uncertainty, we found no evidence for greater moisture loss, or greater total mass change, for the samples momentarily exposed to higher %RH conditions during air dryer system maintenance in PF-4 (Figure 2; Appendix 1). A sample from

Lot 36 (UPOPLOT036-2) was deliberately left exposed to relatively high moisture conditions (>10% RH) overnight, but did not gain measurable moisture in excess of that sorbed by a sample handled in the approved manner.

Despite the relatively low gas abundances, offgas spectra are complex and broad with multiple peaks. Typically, ARIES oxides undergo an initial mass loss due to volatilization of adsorbed gases that reaches a maximum between 550 and 790^{o}C (avg. = 629^{o}C, Table 3). The maximum mass loss is ≤ 1.5 mg (avg. = 1.12 ± 0.32 mg). The proportion of weight loss attributable to the devolatilization of sorbed H_2O varies from <10% to over 70%, averaging 34.1% (Appendix 1). Typical moisture contents for processed ARIES UPOPLOT PuO_2 are less than 0.01 wt. % H_2O, and, again using the assumptions in Haschke and Ricketts [9], correspond to ~1 monolayer of H_2O on the oxide surface. The latter result is consistent with the low surface area of the material and the very arid conditions maintained inside the PF-4 glovebox line.

Besides H_2O, other volatile peaks always present in the offgas from ARIES DMO oxides include H_2, CO_2, and NO (Table 3, Figure 9). Offgas peaks occur at remarkably consistent temperatures for various species (Table 3), though the magnitudes vary greatly from sample-to-sample (Appendix 5). Typically, H_2O and CO_2 peak areas are about equal in area and temperature range, while the NO and H_2 peak areas are much smaller in magnitude and less broad. The H_2O release typically show maxima at ~170 and 300^{o}C, suggesting that H_2O may not be simply physisorbed. Forty-five of the 59 samples (76%) have two discrete H_2O peaks; one at low temperature and a higher temperature one approximately 131°C apart (Table 3). Other offgas constituents have maxima at ~160-170°C (NO), ~280-300^{o}C (CO_2 and H_2), and 470-480^{o}C (CO_2). All samples show multiple CO_2 peaks. The lowest temperature CO_2 peak (296.5±12.3°C) coincides with the higher temperature H_2O peak (299.9±26.1°C), and with the H_2 peak (303.7±10.4°C). NO peaks are present in all samples, and typically coincide with the low temperature H_2O emission (167.6±25.1°C). The diatomic hydrogen peak is apparent at ~300^{o}C in all but two of the UPOPLOT samples, though 39% of the samples also display a higher temperature H_2 peak at 440.4±12.6°C.

The great majority of the UPOPLOT samples experienced weight gain following weight loss due to volatilization (Figure 9). Samples showing little or no weight gain include those from the most recent lots, starting with UPOPLOT 39: these are the same samples that showed anomalous PSDs relative to the other UPOPLOT samples. Following the initial mass loss, nearly all ARIES oxide samples slowly gain mass at an average rate of 9.0×10^{-4} mg/^{o}C. Between 770 to 1060^{o}C (avg. = 959^{o}C), 71% of the calcined DMO oxides analyzed thus far experience a sharp increase in the rate of mass gain to an average of 2.4×10^{-3}mg/°C (Figure 9). High temperature weight gain seen in most UPOPLOT TGA samples is accompanied universally by a sharp, concomitant drop in oxygen abundance in the offgas (Figure 9). Typically, the signals at *M/z* = 16 and 32 recover as O_2 leaks back into the system after the initial depletion; via either atmospheric incursion into the sample chamber, or via the carrier gas itself as an impurity. In half of the samples analyzed, the magnitude of the high temperature mass gain (avg. = 0.23±0.16 mg) exceeded that of the more gradual, lower temperature mass gain (avg. = 0.31±0.25 mg). In six of the 59 total DMO oxide samples analyzed for moisture (including duplicates) the combined low- and high-temperature mass gains exceed the total weight lost due to devolatilization.

Appendix 1 summarizes the mass change and moisture data from all processed UPOPLOT TGA-MS runs. If the maximum weight loss is taken as the absolute weight loss of the sample for 3013 purposes, the samples with the greatest mass loss (0.051 wt. %) are still six times lower than the 3013 administrative limit of 0.32 wt. % for moisture alone [2, 5]. Measured water contents of the ARIES UPOPLOT samples analyzed thus far never exceed 0.025 weight %.

DISCUSSION

Specific Surface Area

Early researchers established that the SSA of PuO_2 produced by different methods and then calcined at different temperatures [10-12], could vary by as much as an order of magnitude. These authors observed, as others have subsequently noted [13-14], that the surface area of PuO_2 particles produced by precipitation from solution by any method (e.g., oxalate, nitrate, etc.) decreases quite drastically with increasing calcination temperature. The high surface area of precipitates (e.g., Figure 3) likely has much to do with the intricate, rosette-like, highly convoluted, poly-crystalline surfaces of these materials [8]. Recrystallization at high temperatures tends to eliminate pore spaces and other surface irregularities, resulting in a lower surface area material [10]. Several recent studies summarize SSA data for thermally-stabilized PuO_2 powders [13-14], but do not identify the means by which these powders were produced. The results from previous studies [7, 10, 11] and from the present study indicate that, for PuO_2 powders, different process paths may lead to powders having differing SSAs and PSDs even when calcination temperature does not differ. Thus, an understanding of the process path is an important first step towards ascertaining the physical properties of the bulk powder produced therefrom.

Oxides produced by direct metal oxidation are typically low surface area materials. Moseley and Wing [11] remark specifically on the very low surface area of PuO_2 produced by the direct oxidation of Pu metal in a furnace, but do not provide any data. One sample from the present study, an oxide generated by long term exposure of Pu metal to air at ambient conditions (Appendix 4), is an exception, with an SSA approaching 7 m^2/g. Otherwise, oxides emerging from the ARIES DMO and from the muffle furnace are exclusively low surface area materials, with SSAs typically less than 0.5 m^2/g, which is close to the surface area of spherical grains having a similar particle size range. Scanning electron microscopy of ARIES DMO oxides indicates that some degree of surface area irregularity is apparent in most grains, but very few have the complicated, rosette-like features routinely visible in oxides originally precipitated from the oxalate.

Particle Size Distribution: Reliability of Laser Diffraction Measurements

In terms of PSD, the data from ARIES DMO PuO_2 powder is very consistent. All processed UPOPLOT samples originating from the ARIES DMO furnace have trimodal PSDs, with modes at 0.73 – 3.16 μm, 10.9 – 18.5 μm, and 41.3 - 63.0 μm (Figure 5, Table 2, Appendix 3), as do the particles from the <180 μm populations of the as-received aggregates (Figure 7). Furthermore, PuO_2 retrieved from the static muffle furnace also exhibits a similar tri-modal PSD (Figure 6). Trimodal particle distributions are well-known in nature and have been observed in a wide variety of natural and manufactured materials, including atmospheric aerosols [17], loess and other Aeolian sediments [18-19], chocolate [20], human cough aerosols [21], clays [22],

particulates generated from disc brake wear [23], wire explosions [24], processed wheat flour [25], coal fly ash [26], and uranium foundry operations [27].

The trimodal PSDs observed in the ARIES DMO material are unlike those observed in the oxide generated by long term exposure of Pu metal to air at ambient conditions which are unimodal (1.42 μm) and distributed normally around a median of 1.62 μm (Figure 11). Oxides produced by the firing of Pu oxalate precipitates often have strongly bi-modal PSDs (Figure 11). For oxalate-precipitated, high-purity oxides from the Materials Identification and Surveillance (MIS) Program [8], the primary mode is typically in the 12-14 μm range, with a smaller mode between 0.3 and 3.0 μm. Impure PuO_2-bearing materials produced via oxalate precipitation may also have a third mode at 50-60 μm, though it is very small and is often transient. For high-purity oxides produced by ion exchange of the nitrate solution followed by precipitation as oxalate, the primary mode is in the 30-33 μm range, and the smaller mode is at ~1.5 μm. Thus, PuO_2 produced by oxalate precipitation, by the burning of metal at high temperature, and by the slow oxidation of metal under ambient conditions each possesses a distinct PSD.

The occurrence of trimodal PSDs in materials is attributed to the simultaneous operation of multiple means of particle generation [17, 27]. Within the DMO furnace, oxide is generated directly from metal parts by heating to 475-575°C in an oxygen-rich atmosphere. While the exact temperature of the metal surface is not precisely known, the process is designed to maintain the oxidation temperature below the melting temperature of Pu metal (645 °C), though this may not be the case in practice due to the exothermic nature of Pu metal oxidation. Bulk oxidation of the metal is controlled by the diffusion of oxygen or oxygen-containing species through an oxide layer on the metal surface. The outer surfaces of the metal components oxidize first and spall off, assisted by the tumbling action of the parts in the rotating basket. The spalled-off oxide particles fall through the basket perforations and are conveyed into the screw calciner where they are further oxidized for over two hours at temperatures >1000°C in the same oxygen-rich atmosphere. Thus, oxide particles can be formed in the DMO by several means during oxidation and calcination: combustion, spallation, and fragmentation or comminution. Even though the DMO process was designed to inhibit the melting of Pu, we have seen direct evidence of melt-like droplets and spherules in the as-received oxide (Figure 12), and it is possible that Pu metal vapors or fumes are generated during oxidation. Smaller particles can also undergo coalescence, sintering or coagulation by cold-welding during oxidation, calcination and milling. Some question remains as to how the different means of particle formation would be manifest during oxidation of the metal in a static muffle furnace.

However, it is also possible that artificial trimodal size distributions in wet laser diffraction analyses can arise due to particle flocculation, the assumption of particle sphericity inherent in the optical theory used to construct the diffraction pattern deconvolution algorithms, and the presence of strongly anisotropic particle shapes (e.g., needles) in the sample. These shortcomings of the laser diffraction technique are well-known [28-34], and must be considered when presenting PSD data. Furthermore, PSD data for the same material may vary considerably depending on the measurement technique chosen [33].

The determination of PSD in PuO_2 powders is also problematic for other reasons. Our aim is to ascertain the PSD of the original dry material, as received, using a wet analytical technique

approved for use in a PF-4 glovebox. The material is extremely dense, and larger particles preferentially settle out of aqueous suspension very quickly. The powder contains abundant, loosely-bonded primary particle aggregates formed during calcination by sintering, or mechanically during milling. The propensity for these aggregates to disassemble in the flowing dispersant medium during analysis is expressed as a steady increase in the smallest-size particle mode during analysis (Figure 13), accompanied by a marked increase in laser and light obscuration (Figure 14), and a slight decrease in both the population and the diameter of the larger-sized modes. Figure 13 is a plot of nine individual PSD curves collected over a time span of approximately 9 minutes from a single suspension of a sample from UPOPLOT0005. In this plot, each solid line represents a single particle size analysis. Through time, the larger modes at ~14 and 55 μm are depleted, as the volume percent of particles in the smallest particle size mode grows and moves to a smaller diameter. At the same time, the laser transmittance for each successive analysis decreases from 84.4% to 72.4% (Figure 14). Particles settling out of suspension would tend to increase light transmittance. Thus, some size reduction of primary PuO_2 particle aggregates is apparent during particle size analysis.

It is also possible, conversely, that the observed PSDs for PuO_2 powders are biased by agglomerations formed during analysis via flocculation. Desroches, et al. [34] have shown that such agglomerates can introduce significant bias to PSDs for CeO_2 suspensions in near-neutral solutions. They found that the suspension stability of rare earth- and yttrium-doped CeO_2 powders was enhanced by adjusting the pH of the dispersant medium so it was well outside of the isoelectric point (IEP) of CeO_2, which is close to pH=7. The term “isoelectric point,” also known as the zero point of charge (ZPC), represents the pH at which an immersed solid surface has a zero net charge. The IEP of PuO_2 occurs at approximately pH=9 [35], thus a stable suspension can be generated in a near-neutral solution. As a precaution, we collected PSD data for two splits of the same PuO_2 powder sample in Isoton III dispersant, which has a pH of 7, and in Isoton III that was acidified to pH~4.5 using a few drops of nitric acid. The results of both analyses are within the range expected for routine sample-to-sample variation (Figure 15). For PuO_2, the effect of lowering the pH of the dispersant is modest, but may warrant further systematic investigation. However, the use of a mildly acidic dispersant may cause the internal piping of the laser diffraction instrument to corrode or break down over time.

Particle shape considerations may also come into play for PuO_2 powders from the ARIES DMO. Scanning electron microscopy (SEM) images (Figure 16) indicate that these powders are comprised of particles having aspect ratios that vary from approximately unity to over 4:1. The PuO_2 particles are typically angular and equant, and not spherical in shape, and such particles could certainly be expected to broaden the apparent PSD. While needle-like and plate-like particles can be seen on occasion, they are not the norm. Based on these admittedly crude observations of particle shape, we assume that some bias was potentially introduced into the laser diffraction data by the presence of particles having a large aspect ratio. However, further work will be required before we can address the manner in which such bias is manifest in the final PSD. Similarly, a quantitative assessment of the severity of these effects will require the collection of a corresponding set of particle shape and size distribution data by other means, such as image analysis, on the same samples.

Thermal Analysis

PuO_2 generated via the room temperature oxidation of Pu metal contains a great deal of sorbed H_2O, almost 4 monolayers. Without confirmation by XPS or other analytical means, the manner in which this excess water is sorbed on to the surfaces of this powder remains a topic of speculation.

All ARIES samples undergo an initial weight loss due to the loss of volatiles. TGA-MS analyses indicate that the total amount of H_2O adsorbed onto oxide surfaces is consistently <0.01 wt. % of the total, and constitutes <1 monolayer of surface coverage. For the vast majority of the processed ARIES DMO samples, volatilization and mass loss occurs up to ~630°C, and is followed by a mass gain that sharply changes slope at high temperatures (>900^{o}C). We speculate that the mass gain in these materials proceeds by two distinct mechanisms, one resulting in the gradual, gently-sloping lower-temperature leg (~600-900^{o}C), and another resulting in the more rapid mass gain that typically starts between 900°C and 1000°C. The slope change also corresponds to a sharp depletion of oxygen relative to the other gases present in the furnace atmosphere (Figure 9), and suggests an oxidation reaction is taking place.

We speculate that the gradual, low temperature mass gain is related to the oxidation of non-stoichiometric PuO_{2-x} to a composition closer to ideal PuO_2, or to oxidation of trace impurity elements such as iron. The data do not support the existence of Pu metal in the calcined DMO oxide. TGA-MS experiments on uncalcined DMO oxide that contained tiny amounts of Pu metal all show mass gains starting at temperatures in the 250-350°C range. The magnitude of the mass gain in the metal-bearing runs often exceeds 0.1 wt. %, and obscures the high-temperature mass gain discontinuity seen in most fully-oxidized DMO materials. For calcined and uncalcined oxides containing no Pu metal, the slopes of the lower temperature portion of the mass gain curves are similar and suggest a similar mechanism for mass gain in each. The gradual mass gain between ~600°C and 900°C is accompanied by a similarly gradual decrease in the oxygen signal (Figure 9), some of which could account for the further oxidation of non-stoichiometric PuO_{2-x} to PuO_2. The oxidation reaction happens quite rapidly in the DMO furnace, and it is conceivable that non-equilibrium O-depleted phases formed and small amounts persisted in the interior portions of relatively large granules through the calcination process.

Experimental evidence suggests that the high temperature weight gain associated with the sharp, step-like oxygen depletion (Figure 9) is likely due to the oxidation of gallium. Gallium is an important impurity element in the Pu metal handled by the ARIES process, and is alloyed with plutonium metal to stabilize its δ-phase, making it more malleable and workable. Typical Ga concentrations in the ARIES DMO oxides vary from 5000 to 9000 ppm. White, fibrous films and deposits that formed during TGA analyses on some of the DMO-produced PuO_2 samples (Figure 10), and on the TGA crucible itself, were revealed to be gallium-rich by energy dispersive X-ray fluorescence analysis. Similar coatings were also observed in the DMO furnace, and during experiments on the thermally-induced removal of Ga from Pu metal and oxide [36-37].

Further work here is warranted, as we have not yet confirmed that the Ga-rich white, fibrous phase is, in fact Ga_2O_3. The identity of the white material could easily be accomplished by X-ray diffraction techniques. Furthermore, we have not yet determined whether the precursor to the white fibrous Ga-rich phase is Ga metal or gaseous Ga_2O. If the O_2 potential during the TGA run

is controlled either PuO_2 or by sub-stoichiometric PuO_{2-x}, metallic Ga may persist in equilibrium to relatively high temperatures [38]. The oxidation of Ga would then result in a net weight gain as Ga_2O_3 becomes the equilibrium phase. The mass change discontinuity would then develop as the contrasting reaction kinetics of Ga oxidation overtakes the gradual oxidation of PuO_{2-x}. It is worth noting that similar white films, possibly Ga_2O_3, separated from nearly all of the uncalcined ARIES Pu oxide samples during TGA-MS analysis.

Effects of Changing Oxidation Conditions on Physical Properties of ARIES DMO Oxides
Even in a system as robust and well-characterized as the DMO Furnace, changes in oxidation conditions can lead to measureable changes in oxide properties. Temperatures in the DMO Furnace are monitored and controlled by four thermocouples: North Up Well (NUW), North Low Well (NLW), South Up Well (SUW), and South Low Well (SLW). The furnace uses a control scheme that selects the highest-reading thermocouple to control the furnace temperature to the setpoint. In the initial thermocouple setup, oxidation temperature was controlled by the SLW thermocouple. This thermocouple normally registered the highest temperature of the four temperature probes and was set to read ~500°C, thus providing a temperature ceiling for the remaining three probes. The temperature difference plotted in Figure 17 is the temperature difference between the SLW thermocouple and the lowest-reading thermocouple, initially the NLW, evaluated at the first introduction of oxygen. Upon restart following a maintenance interval during June and July 2012, the temperature controlling capability was routed to the NUW thermocouple, and the SLW became the lowest-reading thermocouple. At this time, we also observed a sharp increase in the temperature differential between the controlling (NUW) and lowest-reading (SLW) thermocouples (Figure 17), from ~40º-80ºC to ~110º-170ºC. This was later diagnosed as resulting from the failure of one of the six furnace heater panels which shifted the thermal dynamics of the furnace during heat-up.

The increased temperature differential likely corresponds to Pu oxidation at somewhat lower temperatures on average, as the temperatures registered by the lowest-reading thermocouple were ~30ºC to 60ºC lower than those of the runs that occurred prior to July 2012. The thermocouples were re-configured in January 2013 to attempt to compensate for the loss of heater capability by taking the NUW thermocouple out of the control loop. This shifted temperature control back to the SLW thermocouple, and reduced the temperature differential back to its original range. SUW is now consistently the lowest-reading thermocouple.

Workers in the ARIES Oxide Processing line immediately noticed a change in the general physical properties of the resulting oxide following the June/July 2012 DMO Furnace maintenance interval. Instead of a black crystalline aggregate dominated by particles and agglomerates >1 mm in diameter, the oxide was a fine yellow-brown powder with relatively few particles over 1 mm in diameter. The processing sieve results from this time period indicate that the weight percent of fine <180 μm particles in the raw, unprocessed oxide increased from ~20-30% to >70% at the same time the heater element malfunction occurred. The bulk density of the oxide generated under the new temperature regime also decreased dramatically to less than 4.0 g/ml from ~5.0 to 5.5 g/ml.

We also observed changes in other physical characteristics of the DMO oxide produced between July 2012 and January 2013. These are summarized in Figure 5, panels A-E of Figure 17, and in

Table 2. The particle size data in both Figure 5 and in Table 2 was averaged over blocks of 10 oxide lots, thereby accentuating the changes in particle size across groups of oxide lots. Figure 17 contains plots of various physical parameters for each processed lot (SSA, volume % of particles <5 μm in diameter, the smallest particle size mode, and median particle size), and selected thermal parameters for the same samples (% total weight change, and % weight gain after the minimum), comparing each with a plot of temperature difference between the control thermocouple and the lowest temperature reading for each run. The parameters that are the most sensitive to the changes in DMO thermal conditions, depicted as the change in temperature differential, appear to be surface area (Figure 17 A), the volume percent of fines (Figure 17 B), the magnitude of the smallest particle size mode (Figure 17 C), and the total percent weight change of the TGA sample (Figure 17 E). Median and mean particle size, however, seem to be relatively insensitive to the change in oxidation conditions, though the averaged data (Figure 5, Table 2) show significant decreases in both. If, as surmised above, Pu metal oxidation occurred at slightly lower temperatures between July 2012 and January 2013, it is possible that the changing thermal conditions in the DMO Furnace corresponded to significant changes in the nature of the Pu oxide product.

CONCLUSIONS

Fifty-plus lots into the ARIES / UPOP production schedule, the characterization data provides strong evidence for a remarkably consistent PuO_2 product in terms of its thermal and physical properties. Further work must be done on the characterization of Pu oxides from different process streams to develop a diagnostic picture of their physical and thermal properties vis-a-vis their processing history. Such data may be applied in the nonproliferation arena to assess the capabilities of rogue nuclear-capable countries. We can draw several conclusions from the data set presented here:

1) PuO_2 generated in the ARIES DMO furnace from Pu metal is consistently a low-surface area material, with SSA values that vary between 0.1 and 0.5 m^2/g.

2) Processed ARIES PuO_2 typically has a bimodal or trimodal PSD. The same can be said of unprocessed PuO_2 fines having diameters less than 180 μm, and of oxide generated in dry air in a standard muffle furnace.

3) PSD and SSA are functions of the thermal and oxidation conditions within the ARIES DMO Furnace, and process upsets may be reflected as observable changes in the physical properties of the PuO_2 product. Changes in PSD are especially apparent when the entire range of particle sizes emerging from the DMO Furnace is considered.

4) ARIES DMO oxide typically has a very low volatile content. Moisture contents are well below the minimum required in DOE-STD-3013-2012.

5) Other gases detected in the offgas from ARIES DMO oxides include CO_2, NO, and H_2.

6) ARIES oxides typically undergo a weight loss, but then gain weight above ~600°C. Above ~900°C, weight gain is attributable to the oxidation of either Ga metal alloyed

with the Pu, or Ga_2O that originated from the alloyed Ga metal. The oxidation of PuO_{2-x} may also occur, causing a gradual weight gain at lower temperatures (600 – 900°C).

ACKNOWLEDGEMENT

This work was funded by the MOX Irradiation, Feedstock, and Transportation budget from the NNSA – NA - 26 (The Office of Fissile Materials Disposition) to LANL for the production of 2 MT of feed for the MFFF. The author thanks Margaret Schwenker, DOE Federal Program Manager, for continued institutional support; Paul DeBurgomaster, Larry Peppers, Kirk Veirs and John Berg for suggesting improvements to the original version of this manuscript; and Harvey Decker, Carl D. Martinez, Richard Salazar, Judy Roybal, Daniel Garcia, Aaron Martinez, and Felix Valdez for ARIES Process Operations. This paper also benefitted from discussions with Larry Peppers, Elizabeth Bluhm, Steve McKee, Kane Fisher, and Blair Art regarding DMO Furnace operations, past and present.

REFERENCES

[1] - ICD-08-025-02, G-ESR-K-00039: “Los Alamos National Laboratory – Savannah River Site (K-Area Complex and/or Mixed Oxide Fuel Fabrication Facility) Plutonium Dioxide Powder Interface Control Document (Rev. 3, 1/31/2013)”

[2] DOE-STD-3013-2012, “DOE Standard: Stabilization, Packaging, and Storage of Plutonium-Bearing Materials,” Department of Energy Technical Standards Program Web Site: http://www.hss.energy.gov/NuclearSafety/ns/techstds/, pp. 1-75, March 2012.

[3] D. E. Wedman, “ARIES Demonstration Report,” LANL Classified Report LA-CP-02-449, 10-03-2002.

[4] D. M. Wayne, “Physical and Chemical Characterization of Bulk ARIES PuO_2 Powders: The Effects of Sieving, Milling, and Blending,” LANL Unclassified Report LA-UR-09-01367, pp. 1-25, 2009.

[5] O. W. Gillispie, L. G. Peppers, E. A. Bluhm, D. M. Wayne, E. J. Kelly, “LANL Response to SRS Requirement G-ESR-G-00035 Item 13, Glovebox Control Between Stabilization, Sampling, and Packaging, and Item 14, Basis for Moisture Measurement, R 1.0” LANL Unclassified Report LA-UR-09-02404, pp. 1-29, 2009.

[6] J. Wang and B. McEnaney, “Quantitative calibration of a TPD-MS system for CO and CO, using calcium carbonate and calcium oxalate,” Thermochimica Acta, 190, pp 143-153, 1991.

[7] J. L. Alwin, F. Coriz, J. A. Danis, B. K. Bluhm, D. M. Wayne, D. W. Gray, K. B. Ramsey, D. A. Costa, E. A. Bluhm, A. E. Nixon, D. J. Garcia, J. D. Roybal, M. T. Saba, J. A. Valdez, D. Martinez, J. R. Martinez, C. M. Martinez, Y. A. Martinez, C. D. Martinez “Plutonium oxide polishing for MOX fuel fabrication” J. Alloys Compounds, 444–445, 565–568 (2007).

[8] D. K. Veirs, “Gas generation from water adsorbed onto pure plutonium dioxide powder” Materials Research Society Symposium Proceedings, 893, 343-348 (2006).

[9] John M. Haschke, Thomas E. Ricketts, “Adsorption of water on plutonium dioxide,” Journal of Alloys and Compounds 252, 148–156 (1997).

[10] K. E. Francis and R. G. Sowden, “The Microstructure of Plutonium Dioxide Prepared by Various Methods.” Chemistry Division, U. K. A. E. A. Research Group, Atomic Energy Research Establishment, Harwell, UK, Unclassified Report AERE-R2939, June 1959, 25 p.

[11] J. D. Moseley and R. O. Wing, “Properties of Plutonium Dioxide,” USAEC Report RFP-503, Rocky Flats Division, Dow Chemical Corporation, Golden, CO, August 24, 1965, 30 p.

[12] O. R. H. Rasmussen, “Ceramic Properties of PuO_2” Atlantic Richfield Hanford Company Unclassified Report ARH-1153, March 25, 1969, 37 p.

[13] J. L. Stakebake, “Determination of Plutonium Dioxide Surface Areas from X-Ray Crystallite Sizes,” J. Catalysis 78, 477-481 (1982).

[14] X. Machuron-Mandard, C, Madic, “Plutonium dioxide particle properties as a function of calcination temperature” J. Alloys Compounds, 235, 216-224 (1996).

[15] C. S. Leasure, D. R. Horrell, R. E. Mason, “Conditions and Results from Thermal Stabilization of Pure and Impure Plutonium Oxides for Long-Term Storage at Department Of Energy Sites” LANL Unclassified Report LA-UR-99-3526, pp. 1-20, (1998).

[16] M. L. Crowder, J. M. Duffey, R. R. Livingston, J. H. Scogin, G. F. Kessinger, P. M. Almond, “Moisture and surface area measurements of plutonium-bearing oxides,” J. Alloys Compounds, 488/2, 565-567 (2009).

[17] K. T. Whitby, “The Physical Characteristics of Sulfur Aerosols” Atmos. Environ., 12, 135-159 (1978).

[18] W. Zhang, C. Dong, L. Ye, H. Ma, L. Yu, “Magnetic properties of coastal loess on the Midao islands, northern China: Implications for provenance and weathering intensity” Palaeogeo. Palaeoclim. Palaeoecol., 333-334, 160–167 (2012).

[19] B.A. Maher, J.M. Prospero, D. Mackie, D. Gaiero, P.P. Hesse, Y. Balkanski, “Global connections between aeolian dust, climate and ocean biogeochemistry at the present day and at the last glacial maximum” Earth Sci. Rev., 99, 61–97 (2010).

[20] E. O. Afoakwa, A. Paterson, M. Fowler, “Factors influencing rheological and textural qualities in chocolate: A review” Trends Food Sci. Tech., 18, 290-298 (2007).

[21] G. Zayas, M.C. Chiang, E. Wong, F. MacDonald, C.F. Lange, A. Senthilselvan, M. King, “Cough aerosol in healthy participants: fundamental knowledge to optimize droplet-spread infectious respiratory disease management” BMC Pulmonary Medicine, 12:11 (2012).

[22] X. Tan, G. Zhang, H. Yin, A.H. Reed, Y. Furukawa “Characterization of particle size and settling velocity of cohesive sediments affected by a neutral exopolymer” Int. J. Sed. Res., 27, 473-485 (2012).

[23] J. Wahlstrom, L. Olander, U. Olofsson “A Pin-on-Disc Study Focusing on How Different Load Levels Affect the Concentration and Size Distribution of Airborne Wear Particles from the Disc Brake Materials” Tribol. Lett., 46, 195–204 (2012).

[24] Y.S. Kwon, AP. Ilyin, A.N. Grigoriev, D.V. Tikhonov “Dynamics of Particles Formation of Metals and their Compounds During the Electrical Explosion of Wires” KORUS 2004 Conference Proceedings, IEEE, June/July 2004, Vol.3, pp.110-112.

[25] W. Kim, S.G. Choi, W.L. Kerr, J.W. Johnson, C.S. Gaines “Effect of heating temperature on particle size distribution in hard and soft wheat flour” J. Cereal Sci., 40, 9–16 (2004).

[26] W.S. Seames “An initial study of the fine fragmentation fly ash particle mode generated during pulverized coal combustion” Fuel Proc. Tech., 81, 109–125 (2003).

[27] A. A. Plionis, D. S. Peterson, L. Tandon, S.P. LaMont “Alpha spectrometric characterization of process-related particle size distributions from active particle sampling at the Los Alamos National Laboratory uranium foundry” Actinides 2009, IOP Conference Series: Materials Science and Engineering 9 (2010) 012041.

[28] E. Brewer, A. Ramsland “Particle Size Determination by Automated Microscopic Imaging Analysis with Comparison to Laser Diffraction” J. Pharm. Sci., 84, 499-501 (1995).

[29] N. Gabas, N. Hiquily, C. Laguerie “Response of Laser Diffraction Particle Sizer to Anisometric Particles” Part. Part. Syst. Charact., 11, 121-126 (1994).

[30] C. M. G. Heffels, P. J. T. Verheijen, D. Heitzmann, B. Scarlett “Correction of the Effect of Particle Shape on the Size Distribution Measured with a Laser Diffraction Instrument” Part. Part. Syst. Charact., 13, 271-279 (1996).

[31] R. N. Kelly, K. J. DiSante, E. Stranzl, J. A. Kazanjian, P. Bowen, T. Matsuyama, N. Gabas “Graphical Comparison of Image Analysis and Laser Diffraction Particle Size Analysis Data Obtained From the Measurements of Nonspherical Particle Systems” AAPS Pharm. Sci. Tech., 7, 3, Article 69 (2006) (http://www.aapspharmscitech.org).

[32] G. Eshel, G. J. Levy, U. Mingelgrin, M. J. Singer “Critical Evaluation of the Use of Laser Diffraction for Particle-Size Distribution Analysis” Soil Sci. Soc. Am. J., 68, 736–743 (2004).

[33] A. Califice, F. Michel, G. Dislaire, E. Pirard “Influence of particle shape on size distribution measurements by 3D and 2D image analyses and laser diffraction” Powder Technology, 237, 67–75, (2013).

[34] M. J. Desroches, I. A. Castillo, R. J. Munz, “Determination of Particle Size Distribution by Laser Diffraction of Doped-CeO_2 Powder Suspensions: Effect of Suspension Stability and Sonication.” Part. Part. Syst. Charact. 22, 310–319 (2005).

[35] M. Kosmulski, “Attempt To Determine Pristine Points of Zero Charge of Nb_2O_5, Ta_2O_5, and HfO_2.” Langmuir, 13, 6315-6320 (1997).

[36] D.G. Kolman, M.E. Griego, C.A. James, D.P. Butt, “Thermally induced gallium removal from plutonium dioxide for MOX fuel production,” Journal of Nuclear Materials, 282, 245-254 (2000).

[37] D. P. Butt, Y. Park, T. N. Taylor “Thermal vaporization and deposition of gallium oxide in hydrogen” J. Nucl. Mat., 264, 71-77 (1999).

[38] T. M. Besmann, T. B. Lindemer, “Chemical Thermodynamic Representations of PuO_{2-x} and $U_{1-z}Pu_zO_w$” J. Nucl. Mat., 130, 489-504 (1985).

[39] H.Z. Zhang, Y.C. Kong, Y.Z. Wang, X. Du, Z.G. Bai, J.J. Wang, D.P. Yu, Y. Ding, Q.L. Hang, S.Q. Feng “Ga_2O_3 nanowires prepared by physical evaporation” Solid State Comm., 109, 677–682, (1999).

[40] Z. R. Dai, Z. W. Pan, Z. L. Wang “Gallium Oxide Nanoribbons and Nanosheets” J. Phys. Chem. B, 106, 902-904 (2002).

TABLES

Table 1: Sample types included in this study

Prefix	Source	Mode of Preparation
UPOPLOT	ARIES Production, fully processed, 2010-present	DMO-2 Furnace, calcined to 950°C, sieved, milled, blended oxide.
ARIOX	ARIES Demonstration and Testing, production phase, 2011-2012	DMO-2 Furnace, calcined to 950°C, not processed
AR	ARIES Demonstration and Testing, pre-production, 2009-2010	DMO-2 Furnace, calcined to 950°C, not processed
MFTP	Muffle Furnace Test Plan, 2012	Static oxidation in muffle furnace / ambient air, calcined to 950°C
D2	ARIES 2nd Demonstration	DMO-1 Furnace, minimally processed
D1	ARIES 1st Demonstration	DMO-1 Furnace, minimally processed
006	ARIES Pit Disassembly	passive oxidation in ambient air, no calcination

Table 2: Comparison of averaged UPOPLOT PSD analyses.

Units →	**vol %**	**μm**	**μm**	**μm**	**μm**	**μm**	**μm**
	<5 μm	**max PS**	**mode 1**	**mode 2**	**mode 3**	**median**	**mean**
UPOPLOTS 1-10	22.5	174.6	1.41	14.2	54.4	14.7	23.5
UPOPLOTS 11-20	25.4	174.6	1.08	14.2	54.7	14.9	23.3
UPOPLOTS 21-30	20.2	174.6	1.41	16.2	54.7	17.4	25.9
UPOPLOTS 31-37, 39	22.4	152.5	1.41	16.2	54.5	15.6	23.6
UPOPLOTS 40-50	16.2	152.5	2.79	14.1	42.2	13.2	17.8

Table 3: Average, maximum, and minimum peak temperatures (plus standard deviations and percent relative deviations) for the typical H_2O, CO_2, NO and H_2 gas emissions from 59 processed UPOPLOT samples. Most samples exhibited two water and two CO_2 peaks, plus single NO and H_2 peaks.

	T max wt. loss	**T°C H_2O #1**	**T°C H_2O #2**	**T°C CO_2 #1**	**T°C CO_2 #2**	**T°C NO**	**T°C H_2**
Avg.	603.4	169.0	299.9	296.5	475.8	167.6	303.7
Std.Dev.(1σ)	*90.6*	*15.3*	*26.1*	*12.3*	*28.7*	*25.1*	*10.4*
Max.	875.7	203.3	355.1	334.9	531.3	238.3	338.6
Min.	368.6	139.1	258.6	275.2	424.5	133.1	287.6
% RSD (1σ)	*15.0*	*9.1*	*8.7*	*4.1*	*6.0*	*15.0*	*3.4*

FIGURES

Figure 1: ARIES (Advanced Recovery & Integrated Extraction System) Direct Metal Oxidation (DMO-2) Furnace / Calciner.

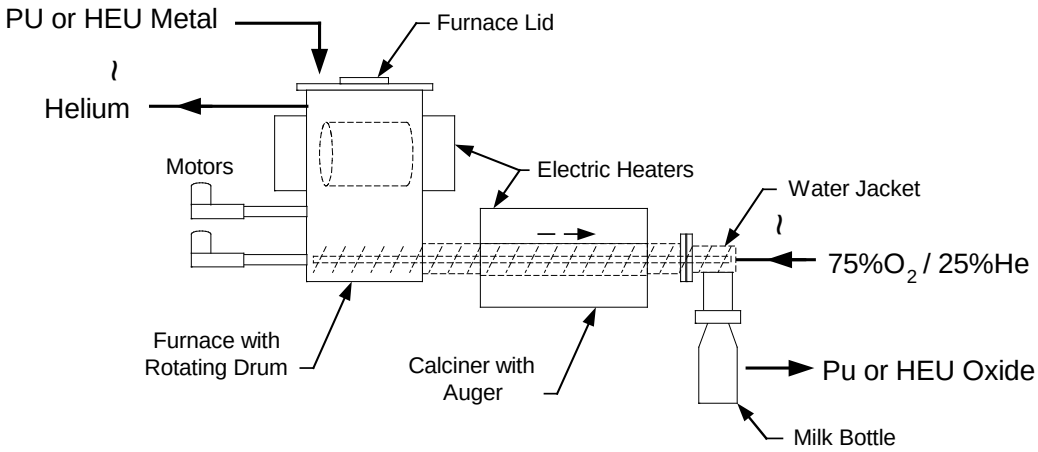

Figure 2: Relative Humidity (lower plot) in the analytical & process gloveboxes versus time. The scatter plot at the top shows the corresponding TGA results (n>50 due to repeat analyses) for total moisture and mass change in TGA samples over the same time period. See Appendix 1 for a complete data summary.

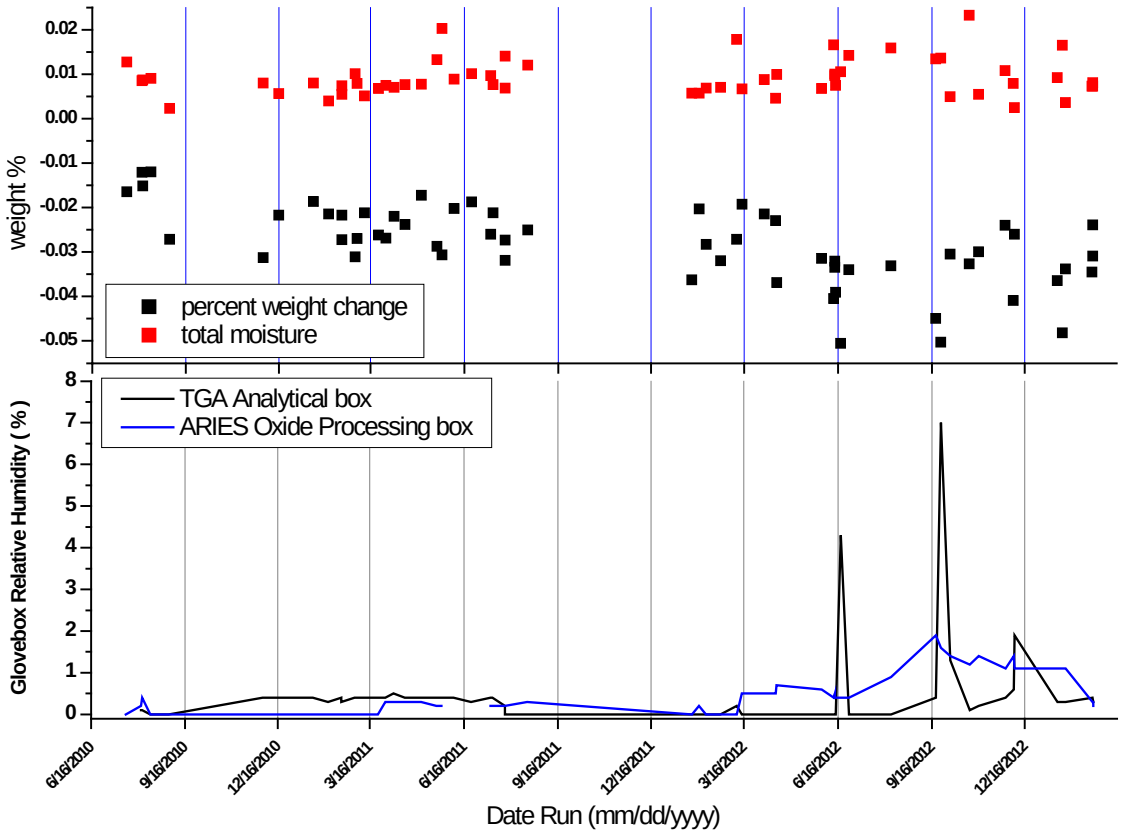

Figure 3: SSA versus total mass change measured by loss-on-ignition (LOI: open symbols) and TGA (solid symbols) for various Pu oxides. Samples from the MOX Pu Polishing Project (open purple circles) and the oxide produced by slow oxidation of the metal in ambient air (solid green diamonds) have considerably greater SSAs than the ARIES-related materials. Processed ARIES "UPOPLOT" DMO-2 oxide (solid blue circles), unprocessed ARIES DMO-2 oxide (solid red squares), and the muffle furnace (MFTP) oxide (solid black diamonds) have very similar SSAs and exhibit very similar mass change behavior in TGA. Oxides from the 2nd ARIES Demonstration created in DMO-1 (open red squares) exhibit a wider range in SSA and positive LOI results, indicating weight gain.

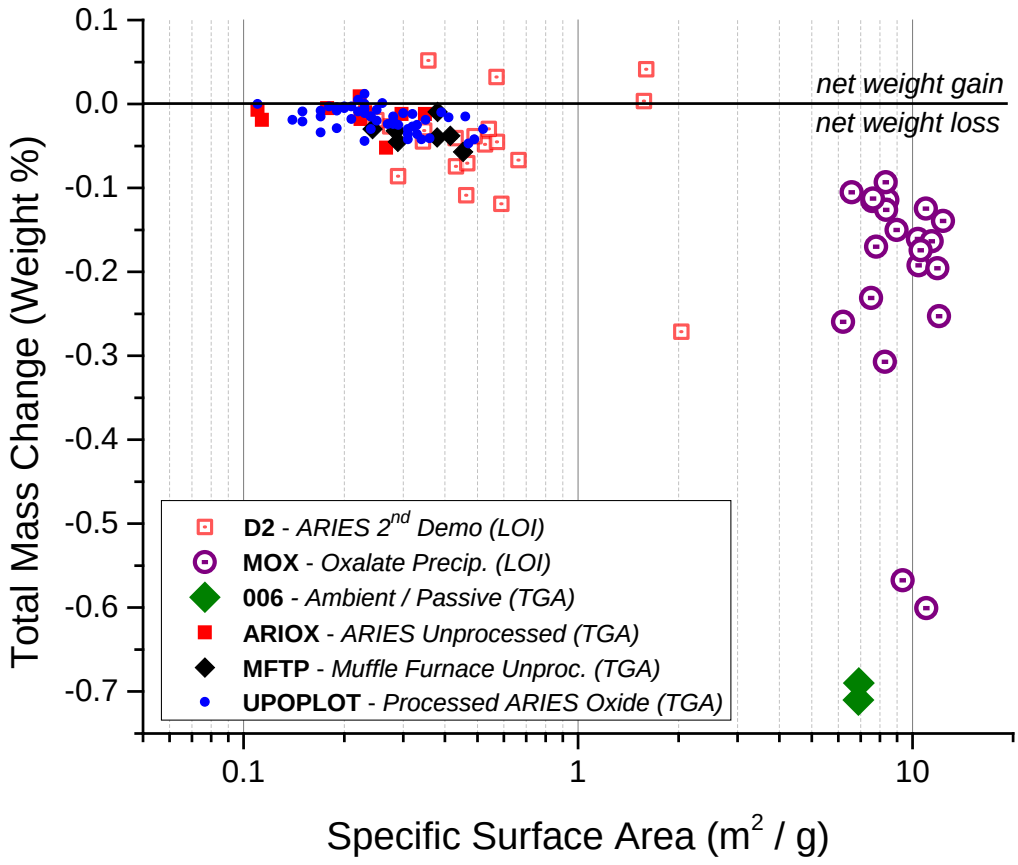

Figure 4: Mean particle size and SSA for the first 53 processed UPOPLOT samples, including duplicates. The shaded area denotes the change in conditions (Lots 40-53) during June/July 2012 that resulted in the alteration of the overall appearance, bulk and tapped density, surface area, and certain particle size parameters of the product oxide (see text).

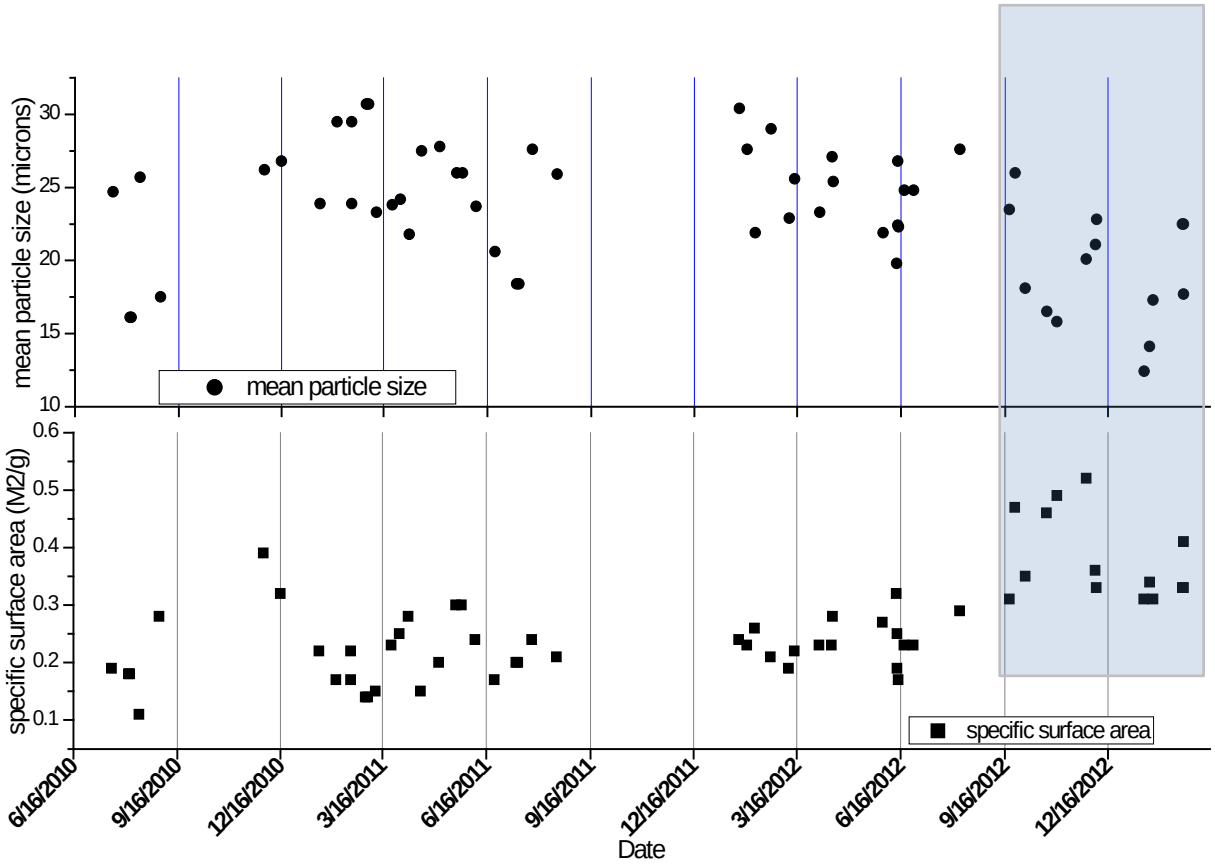

Figure 5: Average PSDs for processed UPOPLOT oxides from ARIES DMO, and the Muffle Furnace Test Plan. Lot 38M is processed Muffle Furnace oxide, and "MF<180 Avg" is the average of all PSDs of all <180 fractions from the unprocessed MFTP oxide. Note that the PSD for Lots 40-50 (magenta line) is substantially different than the others.

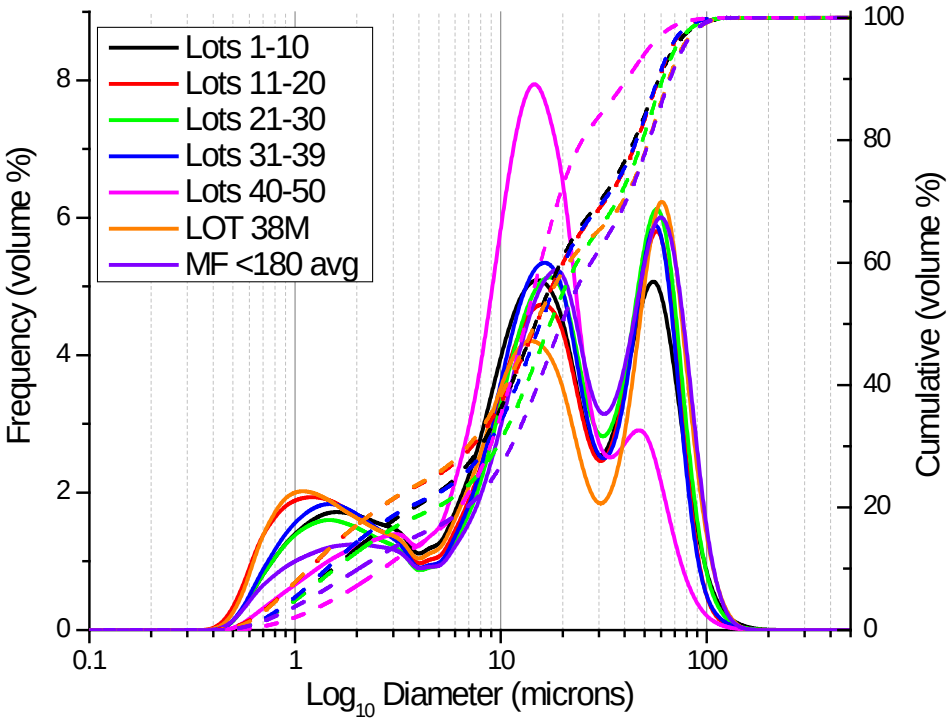

Figure 6: PSDs from the <180 μm fraction of the unprocessed MFTP oxides in comparison to the average particle size of the processed UPOPLOT oxides (navy blue).

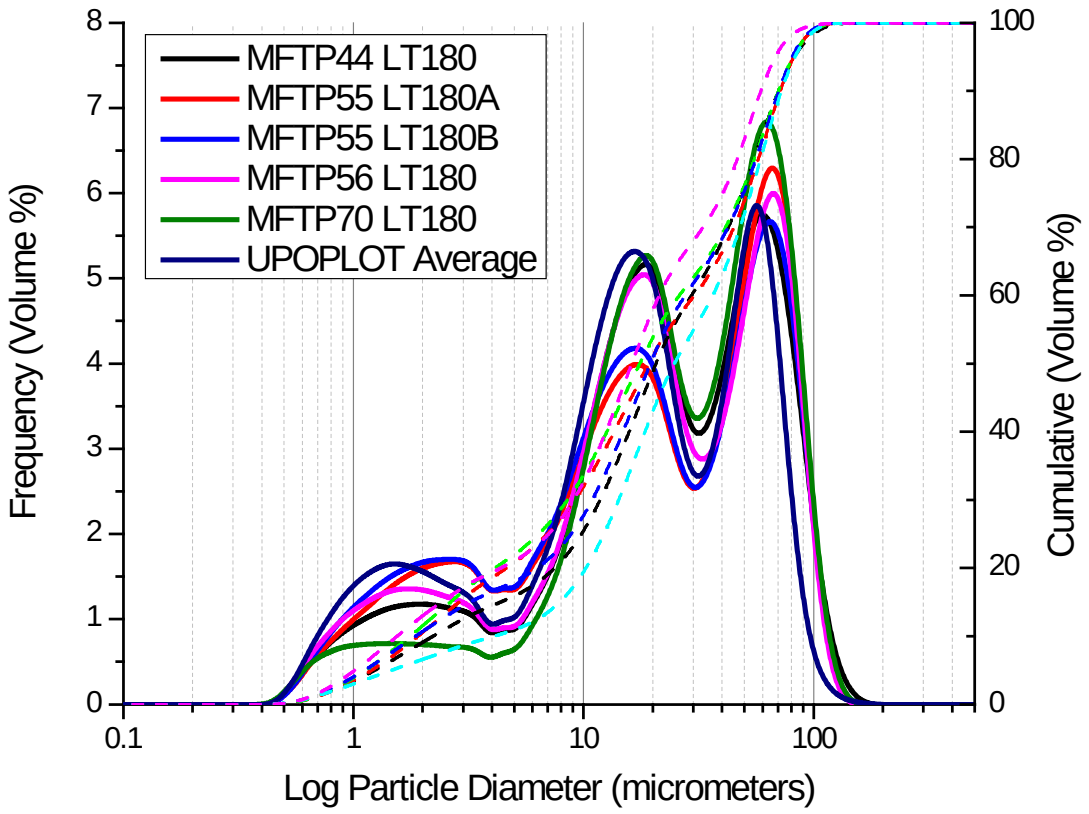

Figure 7: Average PSDs for unprocessed UPOPLOT oxides from ARIES DMO.

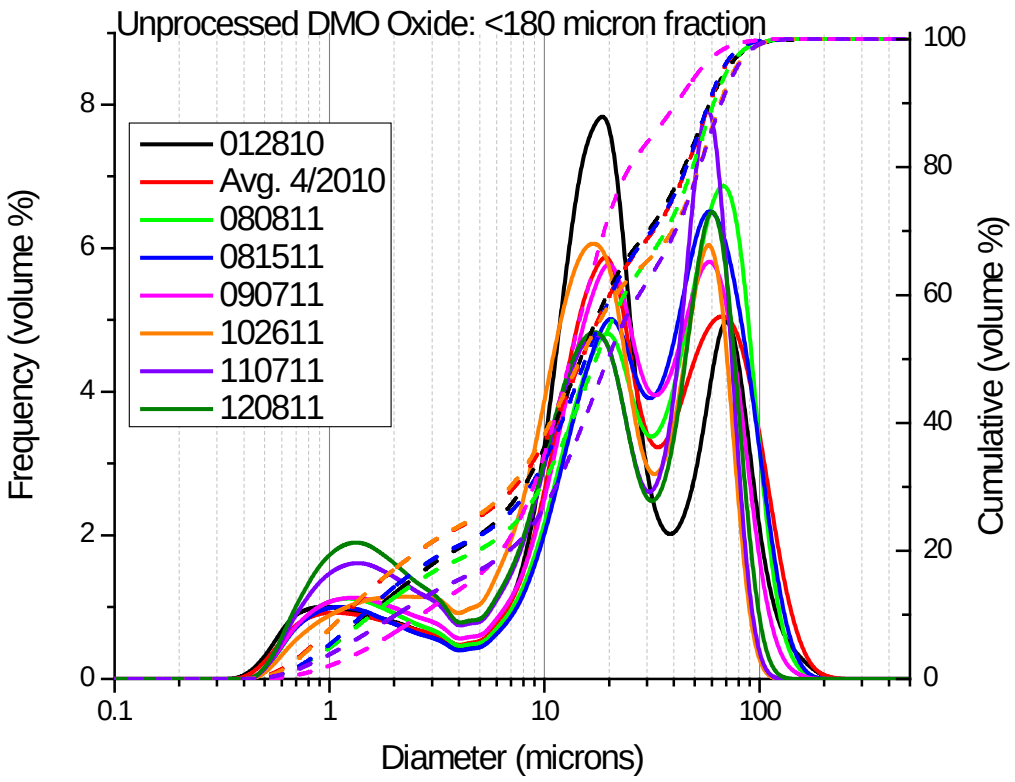

Figure 8: TGA-MS data from PuO_2 generated by long-term (~30 yr.) exposure of Pu metal to ambient air. Using the approximations calculated in [9], the H_2O released corresponds to ~3.7 monolayers for a sample having a SSA of ~7 m^2/g.

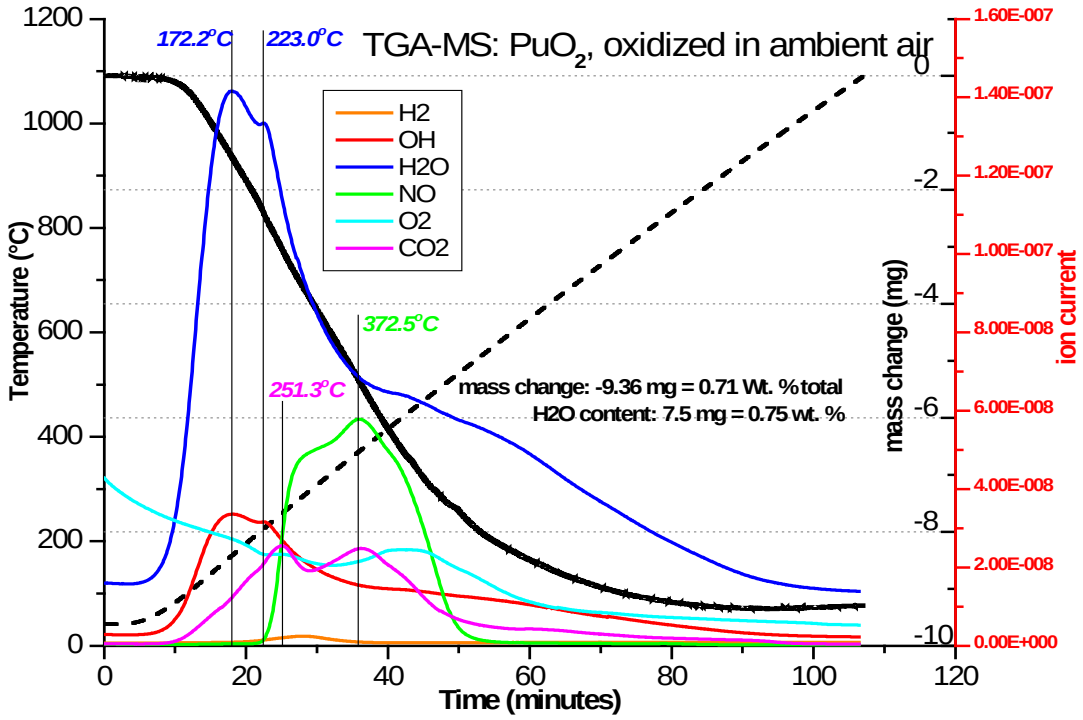

Figure 9: TGA-MS data from fully processed UPOPLOT oxide generated in the ARIES DMO Furnace from Pu metal. Using the assumptions in [9], the amount of moisture lost (0.31 mg) is equivalent to ~0.92 monolayer of H_2O on the oxide surface (SSA = 0.41 m^2/g, sample weight =3.873 g). Note the mass increase above 624°C, and the coeval mass discontinuity and oxygen (cyan line) depletion at 995°C.

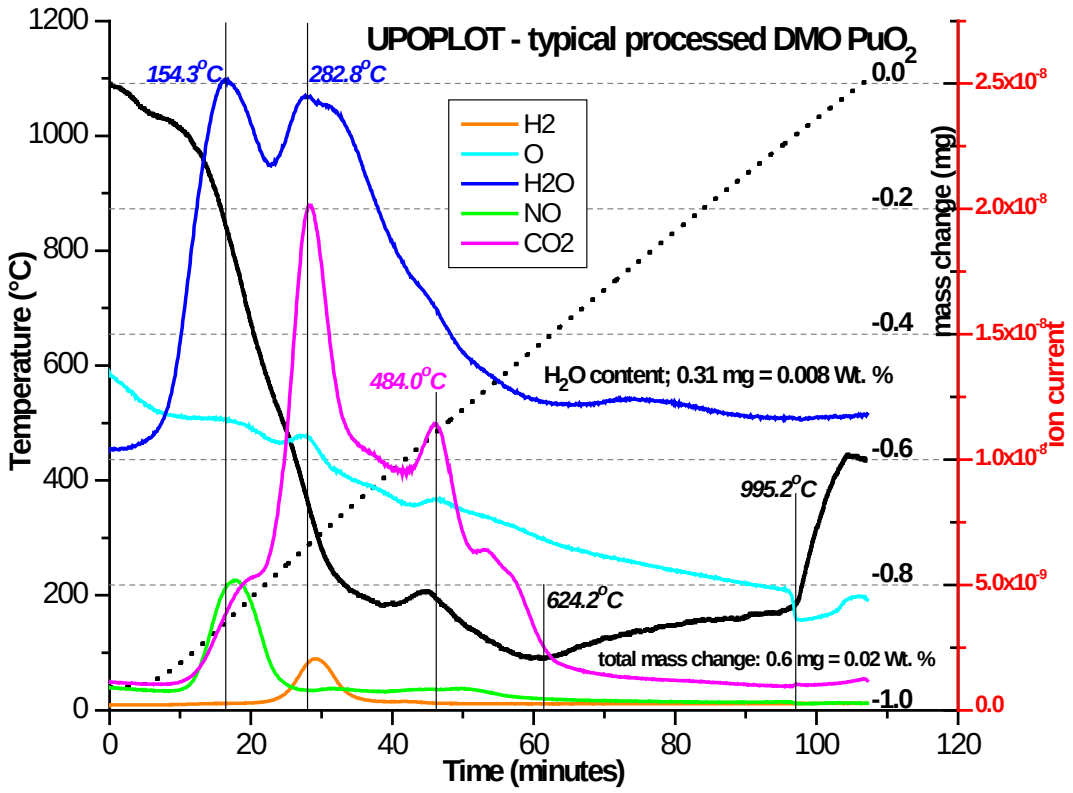

Figure 10: TGA crucible containing a PuO_2 sample, after analysis, showing the white deposits that were later identified as a gallium oxide, probably Ga_2O_3. The crucible is 1 cm in diameter.

Figure 11: PSDs of PuO_2 produced by the slow, passive oxidation of Pu metal under ambient conditions (black curves) and by precipitation from Pu oxalate followed by oxide conversion at 600°C. The red line represents a high-purity oxalate precipitate, and the magenta line represents an impure oxalate precipitate.

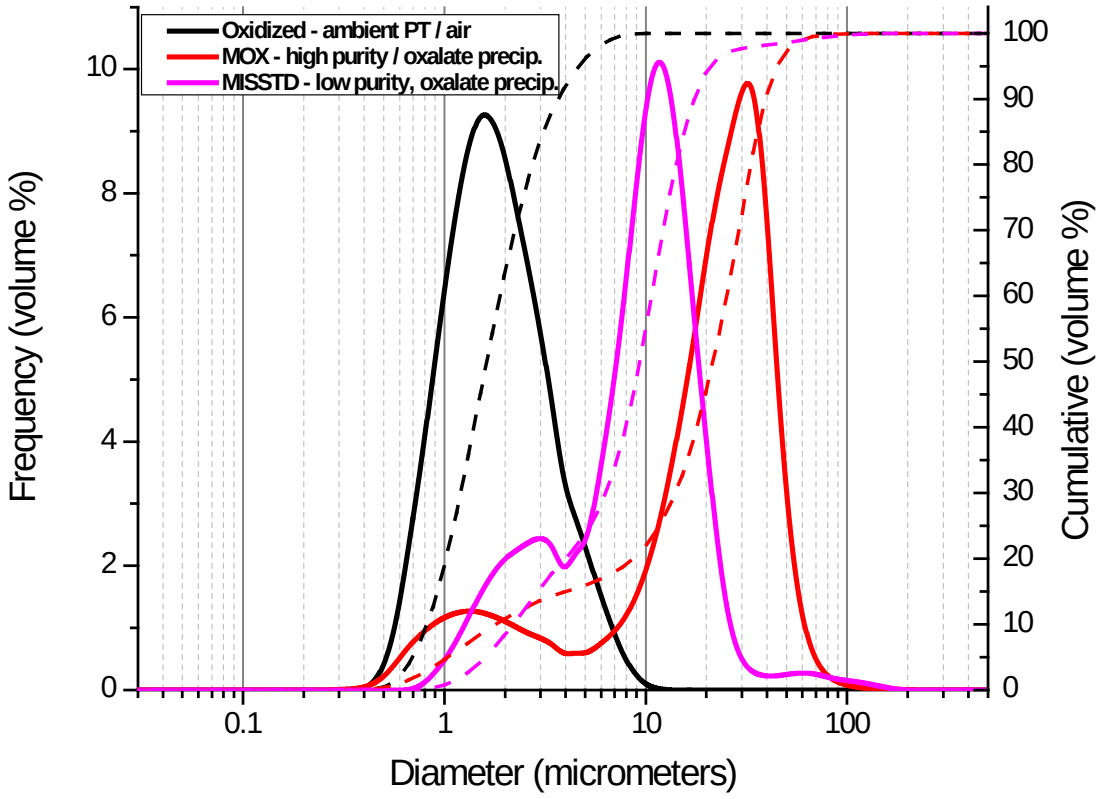

Figure 12: As-received PuO_2 from the ARIES DMO furnace prior to June 2012. Note the presence of oxide spherules in the lower right and center of the picture. The spherules are typically hollow and indicate initial melting of Pu metal into droplets and subsequent oxidation. Calcination to >950°C in an oxygen-rich atmosphere eliminates any metal that passes through the furnace's oxidation segment.

Figure 13: Individual PSD curves from UPOPLOT0005; each solid line represents a single particle size analysis, starting at time=1600 and ending at time=1609. Through time, the larger modes are depleted, as the volume percent of particles in the smallest particle size mode grows and moves to a smaller diameter.

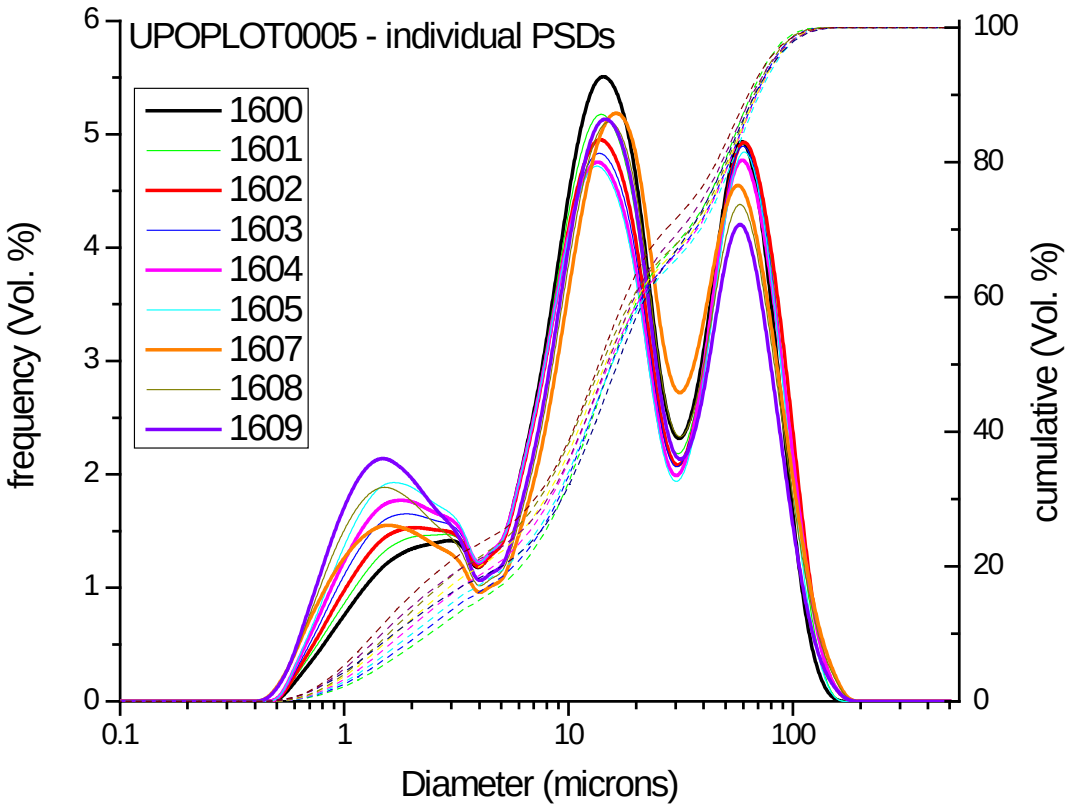

Figure 14: Light transmittance through a suspension of UPOPLOT0005 particle during the acquisition of PSD data depicted in Figure 12.

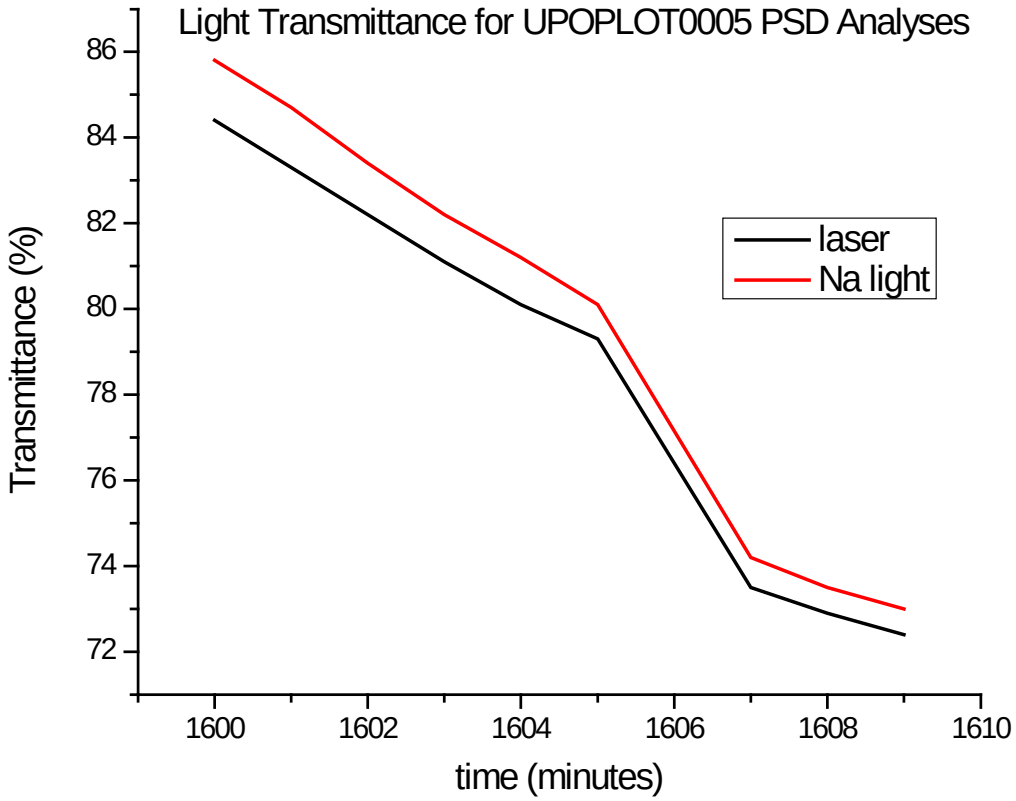

Figure 15: PSDs of two aliquots of the same sample (AR102611) run in dispersants having two different pH levels: near neutral, and slightly acidic.

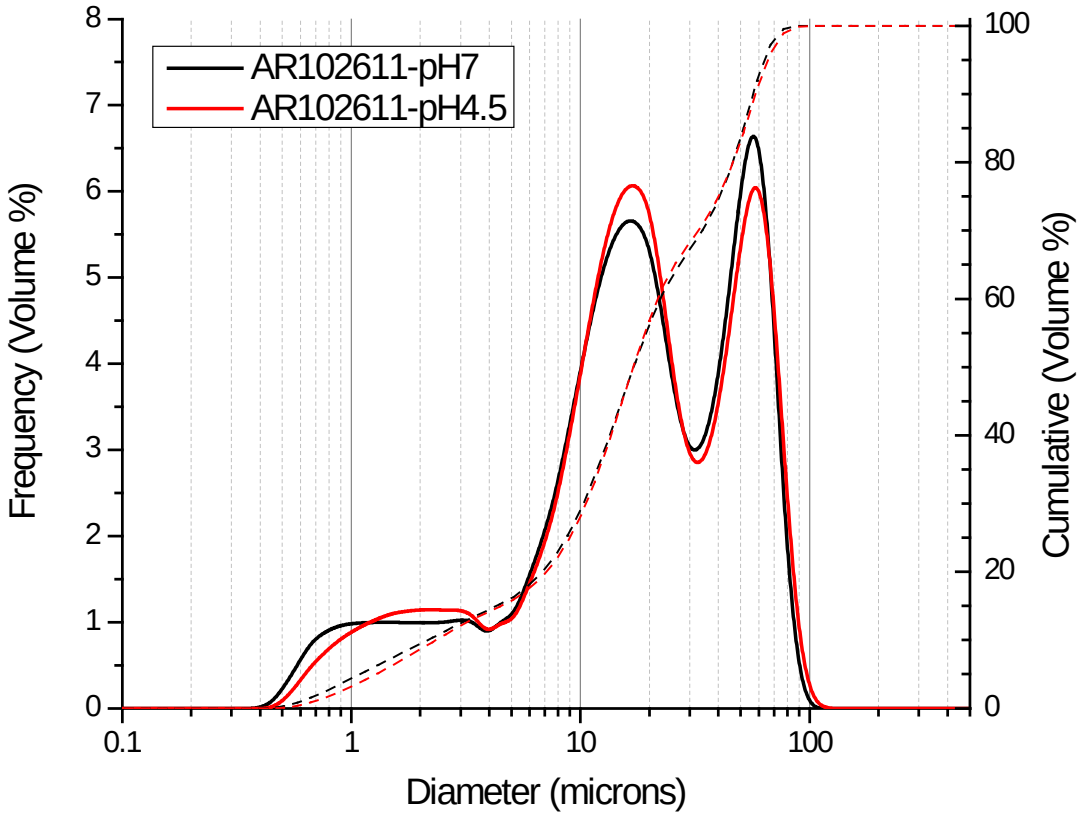

Figure 16: SEM micro-images of unprocessed powder aggregates from the ARIES DMO Furnace.

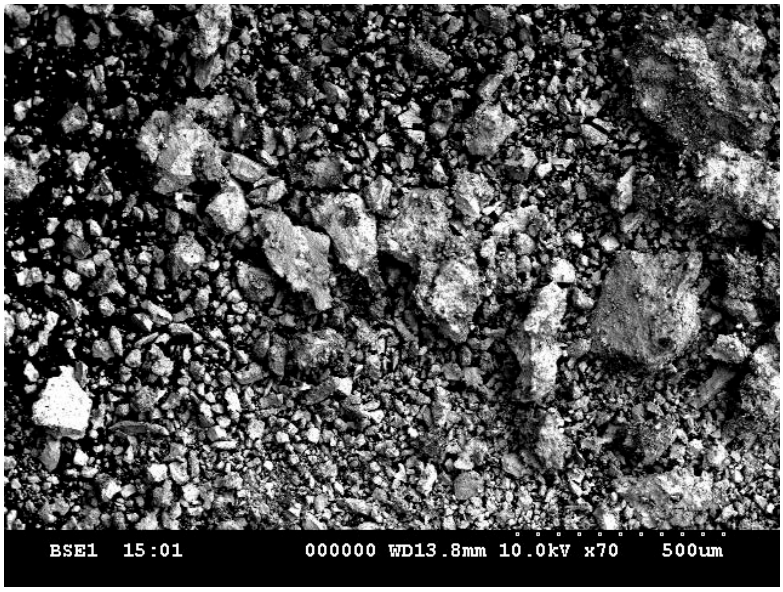

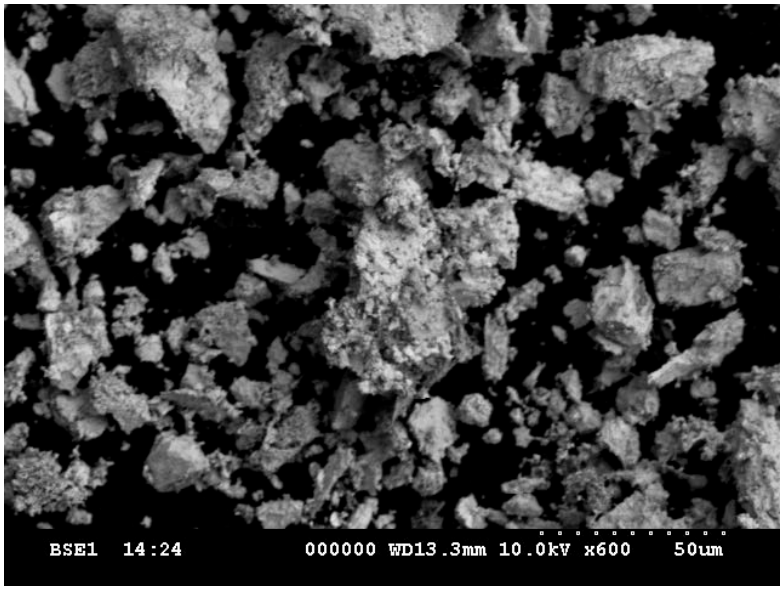

Figure 17: Plots of temperature differential during oxidation in the DMO furnace (black squares) for each batch versus several different physical and thermal properties of the processed oxide. Temperature difference is evaluated at the first introduction of oxygen, and greater temperature differential corresponds to lower metal surface temperature at the start of oxidation. The parameters plotted in comparison to the DMO furnace temperature differential include surface area (A), the volume percent of fines (B), the magnitude of the smallest particle size mode (C), median particle size (D), the total percent weight change of the TGA sample (E, magenta) and total weight gain during TGA analysis (E, violet).

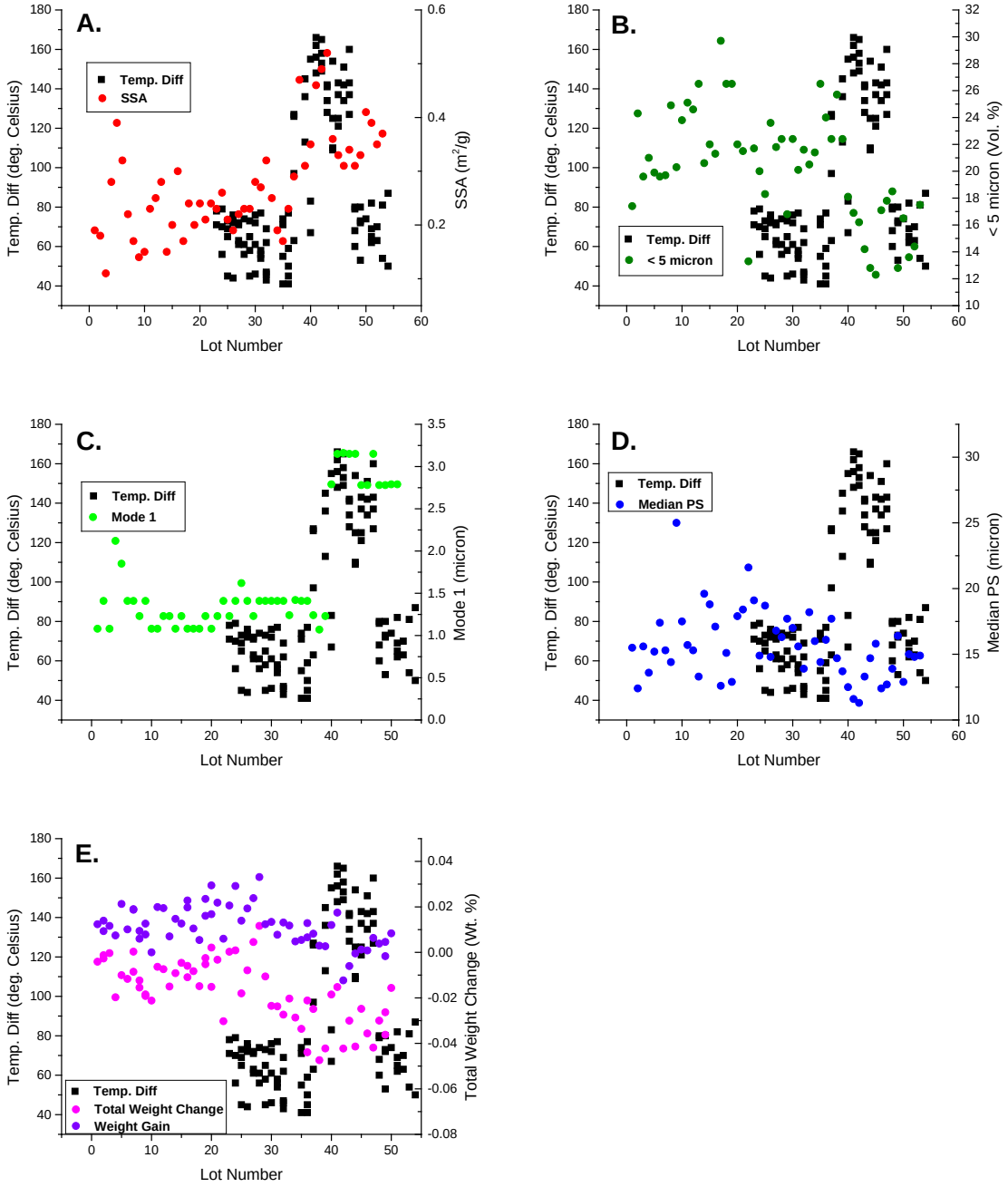

APPENDICES

Appendix 1: Glovebox conditions, mass change, and moisture content data from TGA-MS analyses of processed ARIES DMO PuO_2 samples.

sample	Analytical Box %RH	Process Box %RH	Sample Weight mg	Max Wt. Loss Wt. %	Mass Gain Wt. %	Net Mass Change Wt. %	Total Mois-ture Wt. %	% mass loss due to H_2O %
UPOPLOT0001	--	0.0	3158.9	-0.016	0.012	-0.004	0.013	-77.3
UPOPLOT0002-1	0.1	0.2	3309.9	-0.012	0.009	-0.003	0.008	-70.0
UPOPLOT0002-2	0.1	0.4	3234.2	-0.015	0.014	-0.001	0.009	-57.1
UPOPLOT0003	0.0	0.0	3005.5	-0.012	0.012	0.000	0.009	-75.0
UPOPLOT0004	0.0	0.0	3495.7	-0.027	0.007	-0.020	0.002	-8.4
UPOPLOT0005	0.4	0.0	4884.1	-0.031	0.021	-0.010	0.008	-25.5
UPOPLOT0006	0.4	0.0	3950.0	-0.022	0.010	-0.012	0.006	-25.6
UPOPLOT0007-1	0.4	0.0	3156.1	-0.019	0.019	0.000	0.008	-42.4
UPOPLOT0007-2	0.4	0.0	2458.4	-0.027	0.019	-0.009	0.007	-26.9
UPOPLOT0008-1	0.3	0.0	4840.6	-0.021	0.006	-0.015	0.004	-18.3
UPOPLOT0008-2	0.3	0.0	4780.6	-0.022	0.009	-0.012	0.005	-25.0
UPOPLOT0009-1	0.4	0.0	4275.7	-0.031	0.013	-0.018	0.010	-32.3
UPOPLOT0009-2	0.4	0.0	4328.0	-0.027	0.008	-0.019	0.008	-29.1
UPOPLOT0010	0.4	0.0	4956.4	-0.021	0.000	-0.021	0.005	-23.8
UPOPLOT0011	0.4	0.0	4724.7	-0.026	0.020	-0.006	0.007	-25.8
UPOPLOT0012	0.4	0.3	4724.7	-0.027	0.019	-0.007	0.007	-27.6
UPOPLOT0013	0.5	0.3	4992.2	-0.022	0.007	-0.015	0.007	-31.8
UPOPLOT0014	0.4	0.3	3935.7	-0.024	0.015	-0.009	0.008	-31.9
UPOPLOT0015	0.4	0.3	4574.3	-0.017	0.013	-0.005	0.008	-44.3
UPOPLOT0016-1	0.4	0.2	4381.0	-0.029	0.023	-0.006	0.013	-46.0
UPOPLOT0016-2	0.4	0.2	4304.0	-0.031	0.020	-0.011	0.020	-65.9
UPOPLOT0017	0.3	--	4951.2	-0.019	0.011	-0.008	0.010	-53.8
UPOPLOT0018	0.4	--	4976.2	-0.020	0.005	-0.015	0.009	-43.6
UPOPLOT0019-1	0.4	0.2	4383.3	-0.026	0.023	-0.003	0.010	-36.8
UPOPLOT0019-2	0.4	0.2	4608.8	-0.021	0.016	-0.005	0.008	-35.7
UPOPLOT0020-1	0.2	0.2	4722.6	-0.027	0.029	0.002	0.014	-51.2
UPOPLOT0020-2	0.0	0.2	5008.6	-0.032	0.017	-0.015	0.007	-21.3
UPOPLOT0021	0.0	0.3	4348.3	-0.025	0.022	-0.003	0.012	-47.7
UPOPLOT0022	0.0	0.0	3500.0	-0.036	0.006	-0.030	0.006	-15.7
UPOPLOT0023	0.0	0.2	3541.4	-0.020	0.021	0.000	0.006	-27.8
UPOPLOT0024	0.0	0.0	3394.1	-0.028	0.029	0.001	0.007	-24.0
UPOPLOT0025	0.0	0.0	3160.4	-0.032	0.014	-0.018	0.007	-21.8
UPOPLOT0026	0.2	0.0	3938.7	-0.027	0.019	-0.008	0.018	-65.4
UPOPLOT0027	0.0	0.5	4194.8	-0.019	0.024	0.005	0.007	-34.6
UPOPLOT0028	0.0	0.5	3868.5	-0.021	0.033	0.012	0.009	-41.0
UPOPLOT0029	0.0	0.5	3966.4	-0.023	0.012	-0.011	0.005	-19.8
UPOPLOT0030	0.0	0.7	3655.5	-0.037	0.013	-0.024	0.010	-26.7
UPOPLOT0031	0.0	0.6	4002.5	-0.031	0.008	-0.024	0.007	-21.4
UPOPLOT0032	0.0	0.4	3506.5	-0.040	0.013	-0.027	0.017	-40.8
UPOPLOT0033	0.0	0.5	3736.7	-0.032	0.012	-0.020	0.010	-30.0
UPOPLOT0034	0.0	0.4	3520.8	-0.034	0.005	-0.029	0.010	-29.7
UPOPLOT0035	0.0	0.4	3479.3	-0.039	0.005	-0.034	0.007	-19.1
UPOPLOT0036-1	0.0	0.4	3731.4	-0.034	0.013	-0.021	0.014	-41.7
UPOPLOT0036-2	4.3	0.4	3324.5	-0.051	0.007	-0.044	0.011	-20.8
UPOPLOT0037	0.0	0.9	3655.8	-0.033	0.008	-0.025	0.016	-47.9
MFTP-UPOPLOT0038	7.0	1.6	3755.6	-0.050	0.003	-0.047	0.014	-27.0
UPOPLOT0039	0.4	1.9	3360.0	-0.045	0.003	-0.042	0.013	-29.8

sample	Analytical Box %RH	Process Box %RH	Sample Weight mg	Max Wt. Loss Wt. %	Mass Gain Wt. %	Net Mass Change Wt. %	Total Mois-ture Wt. %	% mass loss due to H_2O %
UPOPLOT0040	1.3	1.4	4321.4	-0.031	0.012	-0.019	0.005	-15.9
UPOPLOT0041	0.1	1.2	4003.2	-0.033	0.017	-0.015	0.023	-71.0
UPOPLOT0042	0.2	1.4	4066.0	-0.030	-0.012	-0.042	0.005	-18.0
UPOPLOT0043	0.4	1.1	3993.2	-0.024	-0.006	-0.030	0.011	-44.8
UPOPLOT0044	0.6	1.4	4179.5	-0.041	0.000	-0.041	0.008	-19.3
UPOPLOT0045	1.9	1.1	4068.7	-0.026	0.001	-0.025	0.002	-9.4
UPOPLOT0046	0.3	1.1	3589.0	-0.037	0.001	-0.036	0.009	-25.2
UPOPLOT0047	0.3	1.1	3464.5	-0.048	0.006	-0.042	0.016	-34.1
UPOPLOT0048	0.3	1.1	3897.3	-0.034	0.004	-0.030	0.004	-10.6
UPOPLOT0049-1	0.4	0.3	4140.1	-0.035	-0.002	-0.036	0.007	-21.0
UPOPLOT0049-2	0.3	0.3	3717.8	-0.031	0.005	-0.026	0.007	-23.5
UPOPLOT0050	0.3	0.2	3837.1	-0.024	0.008	-0.016	0.008	-33.7
AVG			**3983.7**	**-0.028**	**0.012**	**-0.017**	**0.009**	**-34.1**
STD			*591.7*	*0.009*	*0.009*	*0.014*	*0.004*	*16.6*
MAX			5008.6	-0.012	0.033	0.012	0.023	-8.4
MIN			2458.4	-0.051	-0.012	-0.047	0.002	-77.3

Appendix 2: ARIES DMO Oxide Dry Sieving Analyses

The oxide is sieved in 8-inch diameter sieves for one hour on an automatic sieve shaker. We used calibrated sieves with the following mesh sizes (in μm): 2000, 1000, 850, 600, 500, 425, 355, 300, 250, 212, and 180. During the early phases of ARIES DMO testing and demonstration, and during Test Plan A, the oxide was characterized by a relatively even distribution of particle sizes with somewhat higher populations in the 800-1000, 600-800, 300-425, and <180 μm size fractions (Plots 1 and 2). For this oxide, the <180 μm fraction typically constituted <30% by weight of the entire batch, necessitating several sieve / mill iterations during processing.

In August 2011, a mechanical malfunction caused DMO basket rotation to slow or cease entirely. This off-normal condition produced oxide having up to 70 weight % <180 μm fines and ~10 weight % coarse material >850 μm in diameter (Plot 3). As soon as normal DMO furnace operations were restored in September 2011, the PSD of the unprocessed ARIES oxide gradually returned to its former pattern (Plot 3). Oxides produced by static oxidation in a muffle furnace in ambient air were also dominated by <180 μm fines (Plot 3). Muffle furnace oxide contained between 35.7 and 73.4 percent <180 mm fines, by weight, with little or no content above 800 μm.

Milling and sieving tests demonstrate that ~20% of the >1000 μm material is eliminated after one minute of milling, with concomitant increases at smaller-diameter populations. The >1000 micron population is eliminated after 5 minutes, and after 15 minutes of milling, nearly 65% of the material passes through the 180 micron sieve. After 30 minutes, over 95% of the material passes through the 180 micron sieve.

Appendix 2, continued: ARIES DMO Pre-production sieve testing results

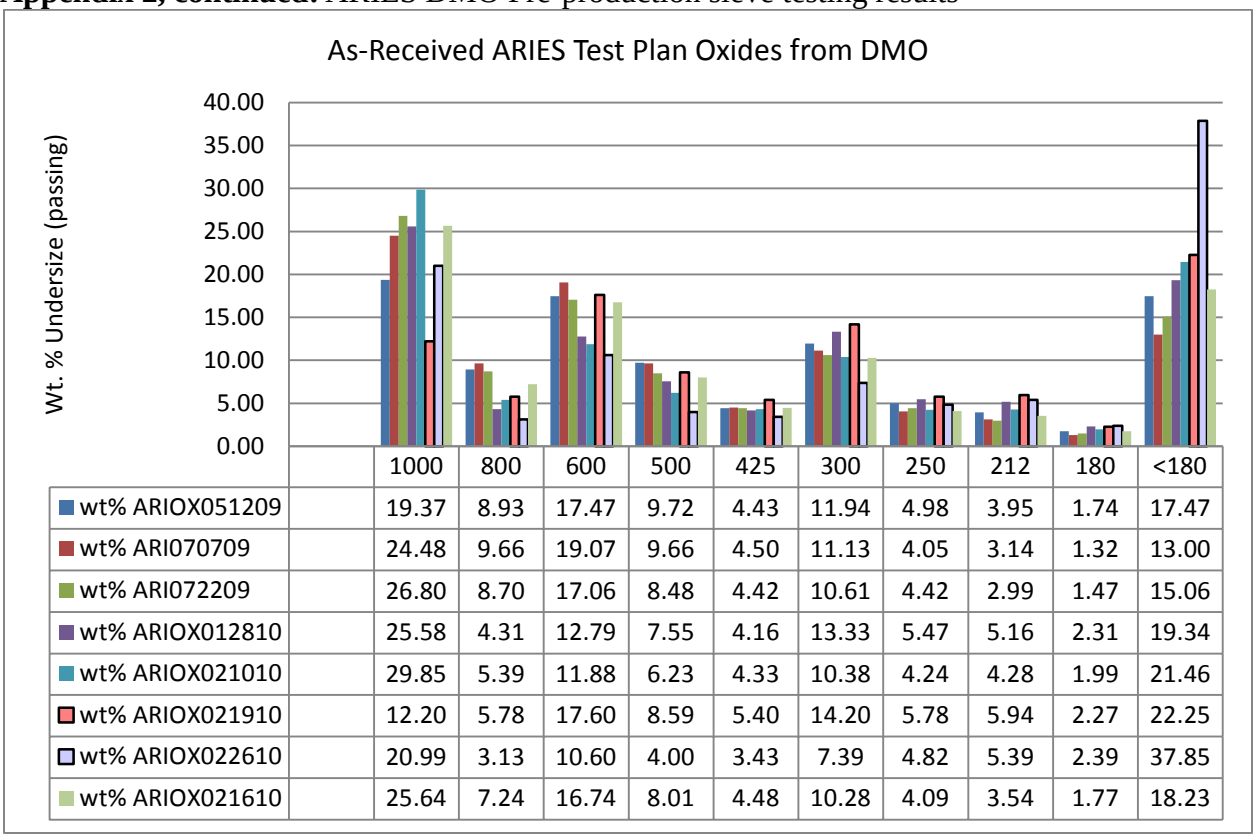

	1000	800	600	500	425	300	250	212	180	<180
wt% ARIOX051209	19.37	8.93	17.47	9.72	4.43	11.94	4.98	3.95	1.74	17.47
wt% ARI070709	24.48	9.66	19.07	9.66	4.50	11.13	4.05	3.14	1.32	13.00
wt% ARI072209	26.80	8.70	17.06	8.48	4.42	10.61	4.42	2.99	1.47	15.06
wt% ARIOX012810	25.58	4.31	12.79	7.55	4.16	13.33	5.47	5.16	2.31	19.34
wt% ARIOX021010	29.85	5.39	11.88	6.23	4.33	10.38	4.24	4.28	1.99	21.46
wt% ARIOX021910	12.20	5.78	17.60	8.59	5.40	14.20	5.78	5.94	2.27	22.25
wt% ARIOX022610	20.99	3.13	10.60	4.00	3.43	7.39	4.82	5.39	2.39	37.85
wt% ARIOX021610	25.64	7.24	16.74	8.01	4.48	10.28	4.09	3.54	1.77	18.23

ARIES DMO Test Plan A sieve testing results

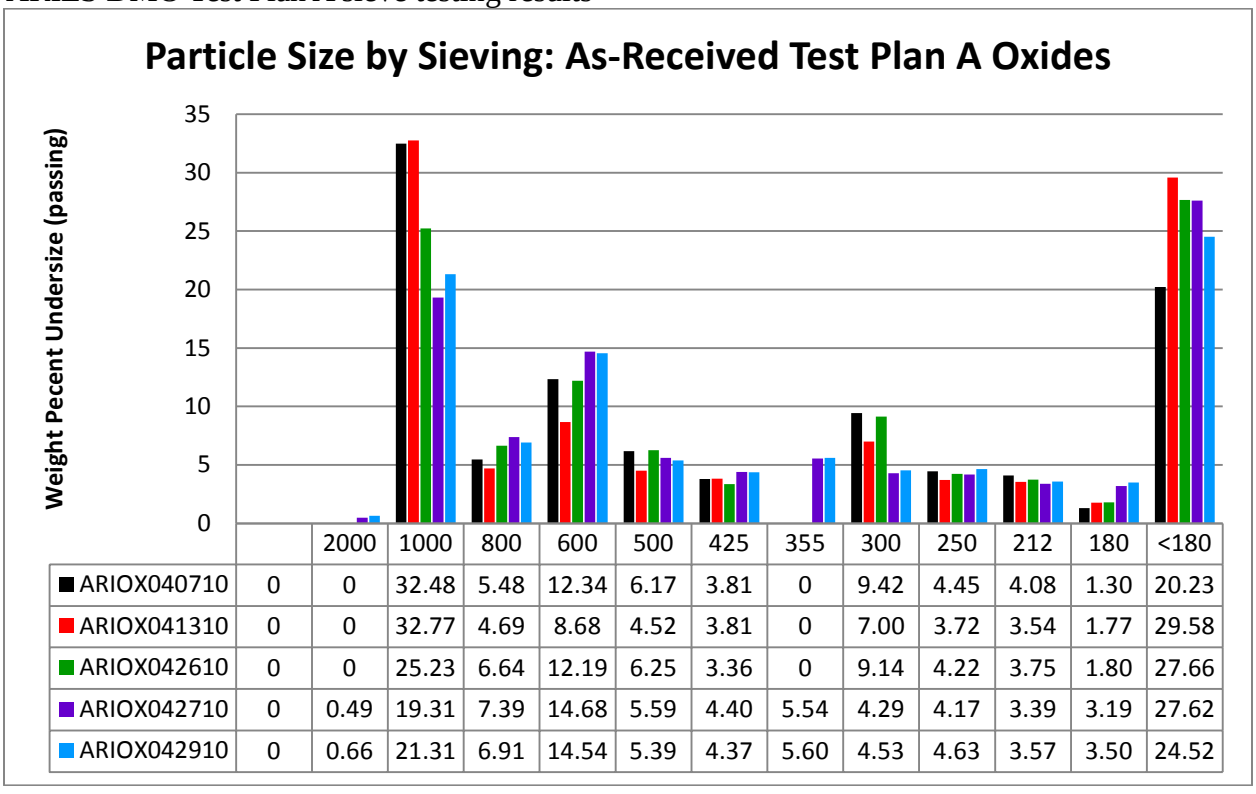

		2000	1000	800	600	500	425	355	300	250	212	180	<180
ARIOX040710	0	0	32.48	5.48	12.34	6.17	3.81	0	9.42	4.45	4.08	1.30	20.23
ARIOX041310	0	0	32.77	4.69	8.68	4.52	3.81	0	7.00	3.72	3.54	1.77	29.58
ARIOX042610	0	0	25.23	6.64	12.19	6.25	3.36	0	9.14	4.22	3.75	1.80	27.66
ARIOX042710	0	0.49	19.31	7.39	14.68	5.59	4.40	5.54	4.29	4.17	3.39	3.19	27.62
ARIOX042910	0	0.66	21.31	6.91	14.54	5.39	4.37	5.60	4.53	4.63	3.57	3.50	24.52

Appendix 2, continued: ARIES DMO (ARIOX) D&T, and Muffle Furnace (MFTP) Sieve Data

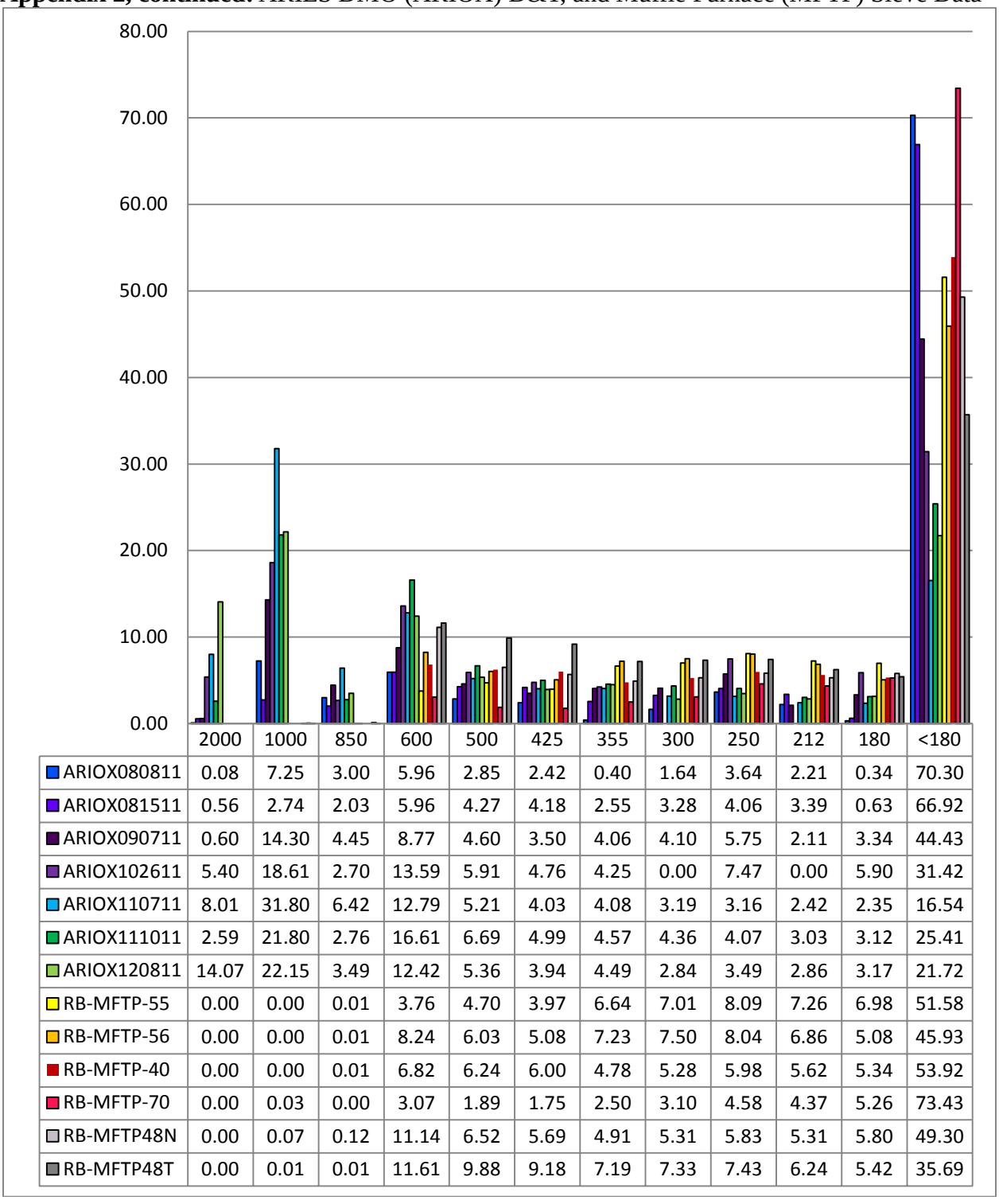

	2000	1000	850	600	500	425	355	300	250	212	180	<180
ARIOX080811	0.08	7.25	3.00	5.96	2.85	2.42	0.40	1.64	3.64	2.21	0.34	70.30
ARIOX081511	0.56	2.74	2.03	5.96	4.27	4.18	2.55	3.28	4.06	3.39	0.63	66.92
ARIOX090711	0.60	14.30	4.45	8.77	4.60	3.50	4.06	4.10	5.75	2.11	3.34	44.43
ARIOX102611	5.40	18.61	2.70	13.59	5.91	4.76	4.25	0.00	7.47	0.00	5.90	31.42
ARIOX110711	8.01	31.80	6.42	12.79	5.21	4.03	4.08	3.19	3.16	2.42	2.35	16.54
ARIOX111011	2.59	21.80	2.76	16.61	6.69	4.99	4.57	4.36	4.07	3.03	3.12	25.41
ARIOX120811	14.07	22.15	3.49	12.42	5.36	3.94	4.49	2.84	3.49	2.86	3.17	21.72
RB-MFTP-55	0.00	0.00	0.01	3.76	4.70	3.97	6.64	7.01	8.09	7.26	6.98	51.58
RB-MFTP-56	0.00	0.00	0.01	8.24	6.03	5.08	7.23	7.50	8.04	6.86	5.08	45.93
RB-MFTP-40	0.00	0.00	0.01	6.82	6.24	6.00	4.78	5.28	5.98	5.62	5.34	53.92
RB-MFTP-70	0.00	0.03	0.00	3.07	1.89	1.75	2.50	3.10	4.58	4.37	5.26	73.43
RB-MFTP48N	0.00	0.07	0.12	11.14	6.52	5.69	4.91	5.31	5.83	5.31	5.80	49.30
RB-MFTP48T	0.00	0.01	0.01	11.61	9.88	9.18	7.19	7.33	7.43	6.24	5.42	35.69

APPENDIX 3: Surface Area and Particle Size Data for processed ARIES UPOPLOT Samples.

Units →	m^2/g	vol %	µm	µm	µm	µm	µm	µm
Sample ID	**SSA**	**<5 µm**	**max PS**	**mode 1**	**mode 2**	**mode 3**	**median**	**mean**
UPOPLOT0001 a	0.19	17.4	116.2	1.08	**14.1**	55.4	15.5	24.7
UPOPLOT0002-S	0.18	24.3	77.3	1.41	**14.2**	41.3	12.4	16.1
UPOPLOT0003-S	0.11	19.6	116.2	1.08	14.1	**62.3**	15.6	25.7
UPOPLOT0004-S	0.28	21	101.5	2.12	**16.2**	42.1	13.6	17.5
UPOPLOT0005-S	0.39	19.9	152.5	1.85	**14.1**	55.1	15.2	26.2
UPOPLOT0006-S	0.32	19.6	200	1.41	16.2	**48.1**	17.4	26.8
UPOPLOT0007-S	0.22	19.7	133.1	1.41	**14.2**	54.9	15.3	23.9
UPOPLOT0008-S	0.17	24.9	200	1.23	12.4	**63**	14.4	29.5
UPOPLOT0009-S	0.14	20.3	116.2	1.41	16.3	**55.1**	25	30.7
UPOPLOT0010-S	0.15	23.8	133.1	1.08	16.3	**42**	17.5	23.3
UPOPLOT0011-S	0.23	25.1	174.6	1.08	16.2	**48.9**	15.7	23.8
UPOPLOT0012-S	0.25	24.6	116.2	1.23	14.2	**55.1**	15.3	24.2
UPOPLOT0013-S	0.28	26.5	101.5	1.23	14.1	**55.6**	13.3	21.8
UPOPLOT0014-S	0.15	20.6	116.2	1.08	16.3	**54.9**	19.6	27.5
UPOPLOT0015-S	0.2	22	152.5	1.23	16.3	**54.6**	18.8	27.8
UPOPLOT0016-S	0.3	21.3	133.1	1.08	16.2	**54.8**	17.1	26
UPOPLOT0017-S	0.17	29.7	88.6	1.08	14.2	**54.1**	12.6	20.6
UPOPLOT0018-S	0.24	26.5	116.2	1.08	16.2	**55.1**	15.1	23.7
UPOPLOT0019-S	0.2	26.5	88.6	1.23	**14.2**	48.1	12.9	18.4
UPOPLOT0020-LO	0.24	22	133.1	1.08	16.2	**55.7**	17.9	27.6
UPOPLOT0021-S	0.21	21.5	101.5	1.23	16.3	**55**	18.4	25.9
UPOPLOT0022-S	0.24	13.3	133.1	1.41	18.5	**54.6**	21.6	30.4
UPOPLOT0023-S	0.23	21.7	133.1	1.23	16.3	**55.2**	19.1	27.6
UPOPLOT0024-S	0.26	20	133.1	1.41	**14.2**	54.7	14.9	21.9
UPOPLOT0025-LO	0.21	18.3	174.6	1.62	16.3	**55.1**	18.7	29
UPOPLOT0026-LO	0.19	23.6	101.5	1.41	14.2	**54.7**	14.8	22.9
UPOPLOT0027-LO	0.22	21.8	133.1	1.23	16.2	**55**	16.8	25.6
UPOPLOT0028-LO	0.23	22.4	101.5	1.41	16.2	**48.6**	16.3	23.3
UPOPLOT0029	0.23	16.8	152.5	1.41	**16.2**	55	17.7	27.1
UPOPLOT0030	0.28	22.4	101.5	1.41	16.2	**54.8**	17	25.4
UPOPLOT0031	0.27	20.1	88.6	1.41	**16.2**	48.7	15.6	21.9
UPOPLOT0032	0.32	21.6	88.6	1.41	**14.2**	48.6	13.9	19.8
UPOPLOT0033	0.25	20.5	116.2	1.24	16.3	**55.5**	18.2	26.8
UPOPLOT0034	0.19	21.4	88.6	1.42	16.2	**48.6**	16	22.4
UPOPLOT0035	0.17	26.5	101.5	1.41	14.2	**54.8**	14.4	22.3
UPOPLOT0036	0.23	24	116.2	1.41	16.2	**55.2**	16.1	24.8
UPOPLOT0037	0.29	22.4	152.5	1.24	16.2	**54.7**	17.7	27.6
MFTP-UPOPLOT0038	0.47	25.7	133.1	1.07	12.4	**55.4**	14.7	26
UPOPLOT0039	0.31	22.4	133.1	1.23	**12.4**	54.7	13.7	23.5

Units →	m^2/g	vol %	µm	µm	µm	µm	µm	µm
Sample ID	**SSA**	**<5 µm**	**max PS**	**mode 1**	**mode 2**	**mode 3**	**median**	**mean**
UPOPLOT0040	0.35	18.1	152.5	2.79	**12.4**	47.8	12.5	18.1
UPOPLOT0041	0.46	16.9	116.2	3.15	**12.3**	48.2	11.6	16.5
UPOPLOT0042	0.49	16.2	101.5	3.16	**10.9**	47.9	11.3	15.8
UPOPLOT0043	0.52	14.2	116.2	3.15	**12.4**	48.6	13.3	20.1
UPOPLOT0044	0.36	12.8	116.2	3.15	**14.2**	48	14.7	21.1
UPOPLOT0045	0.33	12.3	152.5	2.78	**14.2**	48	15.8	22.8
UPOPLOT0046	0.31	17.1	44.9	2.78	**14**	none	12.4	12.4
UPOPLOT0047	0.34	17.8	67.5	3.15	**14.2**	none	12.7	14.1
UPOPLOT0048	0.31	18.5	67.5	2.78	**16.2**	41.6	13.9	17.3
UPOPLOT0049	0.33	12.8	101.5	2.78	**16.2**	48.2	16.4	22.5
UPOPLOT0050	0.41	16.5	133.1	2.79	**12.4**	47.5	12.9	17.7
UPOPLOT0051	0.39	13.6	101.5	2.79	**14.2**	47.9	15	20.1
UPOPLOT0052	0.35	14.4	88.6	2.78	**14.2**	47.9	14.8	20.2
UPOPLOT0053	0.37	17.5	101.5	2.78	**14.2**	48.0	14.9	20.9
UPOPLOT0054	--	15.2	88.6	2.78	**14.2**	48.1	14.5	19.6
AVG	***0.27***	***20.38***	***119.09***	***1.69***	***14.89***	***52.02***	***15.62***	***23.01***
STD	*0.09*	*4.08*	*30.93*	*0.73*	*1.56*	*4.84*	*2.57*	*4.24*
MAX	*0.52*	*29.70*	*200.00*	*3.16*	*18.50*	*63.00*	*25.00*	*30.70*
MIN	*0.11*	*12.30*	*44.90*	*1.07*	*10.90*	*41.30*	*11.30*	*12.40*
%RSD (1σ)	*33.97*	*20.00*	*25.98*	*43.00*	*10.48*	*9.30*	*16.45*	*18.42*

Appendix 4: Physical properties of miscellaneous Pu oxides relevant to the ARIES Program. Prefixes are explained in Table 1. The suffix "LT180" indicates that the sample is the <180 μm sieve fraction of an unprocessed oxide. Positive mass change indicated weight gain during LOI or TGA Analysis.

Sample	Comment	SSA (m^2/g)	% Mass Change (TGA or LOI)	vol % <5 μm	max PS (μm)	mode 1 (μm)	mode 2 (μm)	mode 3 (μm)	D_{50} (μm)	Mean (μm)
006-OX12	Oxidized in ambient air	6.913	-0.658							
006-OX16	Oxidized in ambient air	6.897	-0.707	96.1	11.57	1.42	--	--	1.62	1.99
D1-020906-2	1st Demo unprocessed	0.474		18.4	116.2	0.62	10.8	41.5	14.0	20.3
D1-PSSA1	1st Demo milled	1.219		22.4	152.5	1.41	14.2	--	12.5	15.8
D1-PSSA2	1st Demo milled	1.213		24.5	101.5	1.41	14.1	--	11.4	13.2
D1-PSSA3	1st Demo milled	1.168		21.9	152.5	1.41	14.2	44.8	12.4	16.3
D2-041701SJ	2nd Demo / DMO-1	0.274	-0.027							
D2-042401S5-1	2nd Demo / DMO-1	0.432	-0.074							
D2-042601S5-1	2nd Demo / DMO-1	0.347	-0.032							
D2-042701S5-1	2nd Demo / DMO-1	0.463	-0.109							
D2-043001S5-1	2nd Demo / DMO-1	0.527	-0.048							
D2-061901S5-1	2nd Demo / DMO-1	0.466	-0.071							
D2-062101S5-1	2nd Demo / DMO-1	0.290	-0.086							
D2-070901S5-1	2nd Demo / DMO-1	1.575	0.004							
D2-100401S5-1	2nd Demo / DMO-1	0.571	0.032							
D2-101001S5-1	2nd Demo / DMO-1	0.430	-0.041							
D2-101701S5-1	2nd Demo / DMO-1	0.663	-0.067							
D2-102301S5-1	2nd Demo / DMO-1	0.590	-0.119							
D2-110601S3-1	2nd Demo / DMO-1	0.572	-0.045							
D2-112001S3-1	2nd Demo / DMO-1	0.344	-0.045							
D2-111301S3-1	2nd Demo / DMO-1	0.491	-0.039							
D2-111901S3-1	2nd Demo / DMO-1	0.541	-0.030							
D2-112701S3-1	2nd Demo / DMO-1	2.037	-0.271							
D2-011702S3-1	2nd Demo / DMO-1	0.357	0.052							
D2-040302S2	2nd Demo / DMO-1	0.249	-0.019							
D2-040402S3-1	2nd Demo / DMO-1	1.600	0.042							
AR051209-LT180	ARIES D&T <180 μm	--		14.6	200.0	0.94	16.2	72.1	17.9	32.3
AR070709-LT180	ARIES D&T <180 μm	--		16.2	200.0	0.82	18.4	82.8	21.7	37.4
AR012810-LT180	ARIES D&T <180 μm	--		13.2	200.0	0.82	18.4	63.7	18.0	29.0
AR040710-LT180	ARIES D&T <180 μm	0.305		16.6	133.1	0.94	18.5	55.4	19.1	27.8
AR041310-LT180	ARIES D&T <180 μm	0.288		10.5	152.5	1.23	18.7	72.2	33.5	41.2
AR042910-LT180	ARIES D&T <180 μm	0.208		14.7	152.5	0.82	18.4	72.1	17.9	28.6
AR042610-LT180	ARIES D&T <180 μm	0.296		14.2	229.1	1.23	18.5	48.4	22.4	37.8
AR042710-LT180	ARIES D&T <180 μm	0.255		11.3	152.5	0.82	18.5	55.4	21.0	31.3
AR041310M10	ARIES D&T <180 μm, 10 min. mill	0.212		15.3	133.1	1.08	18.5	62.3	18.5	26.9
ARIOX080811S	ARIES D&T	0.297	-0.012							
ARIOX081511S	ARIES D&T	0.267	-0.052							
ARIOX110711	ARIES D&T	0.110	-0.007							
ARIOX120811	ARIES D&T	0.224	-0.018							
ARIOX102611	ARIES D&T	0.223	0.009							
ARIOX020612S	ARIES D&T	0.113	-0.019							
ARIOX090711U	ARIES D&T	0.178	-0.005							
ARIOX080811-LT180	ARIES D&T <180 μm	0.349	-0.012							
ARIOX090711-LT180	ARIES D&T <180 μm	0.231	-0.010							
MFTP44-LT180	Muffle Furnace <180	0.379	-0.040	15.9	152.4	1.85	18.5	55.2	20.6	30.5
MFTP48N-LT180	Muffle Furnace <180	0.289	-0.045	16.8	101.5	1.23	18.5	61.9	21.3	28.9
MFTP48T-LT180	Muffle Furnace <180	0.243	-0.030	18.6	101.5	1.41	18.4	54.4	18.1	25.3
MFTP55-LT180A	Muffle Furnace <180	0.415	-0.038	20.8	133.1	2.77	16.2	62.9	19.2	30.0
MFTP55-LT180B	Muffle Furnace <180	--	-0.057	21.9	133.1	2.43	16.2	62.7	17.5	28.5
MFTP56-LT180	Muffle Furnace <180	0.453	-0.032	18.0	133.1	1.62	18.4	63.0	19.5	29.7
MFTP62-LT180	Muffle Furnace <180	0.285	-0.009	13.2	88.6	2.11	18.5	48.0	18.2	23.4
MFTP70-LT180	Muffle Furnace <180	0.380	-0.040	10.9	133.1	1.41	18.5	55.5	24.8	33.6